International Institute for
Applied Systems Analysis
IIASA www.iiasa.ac.at

A Time Dependent Zonally Averaged Energy Balance Model to be Incorporated into IMAGE (Integrated Model to Assess the Greenhouse Effect)

Jonas, M., Elzen, M.G.J. den and Olendrzynski, K.

IIASA Collaborative Paper
October 1991

A Time Dependent Zonally Averaged Energy Balance Model to be Incorporated into IMAGE (Integrated Model to Assess the Greenhouse Effect)

Matthias Jonas (IIASA)
Michel den Elzen (RIVM)
Krzystof Olendrzyński (IIASA)

RIVM Report Nr. 222901005
IIASA CP-91-16
October 1991

IIASA
International Institute for Applied Systems Analysis □ A-2361 Laxenburg □ Austria
Telephone: +43 2236 715210 □ Telex: 079 137 iiasa a □ Telefax: +43 2236 71313

rivm
research for man and environment
RIJKSINSTITUUT VOOR VOLKSGEZONDHEID EN MILIEUHYGIENE
NATIONAL INSTITUTE OF PUBLIC HEALTH AND ENVIRONMENTAL PROTECTION
Telephone: 0031 30 749 111 Telex: 47215 rivm nl Telefax: 0031 30 742 971

ABOUT THE AUTHORS

Matthias Jonas is a postdoctoral scholar of the German Research Council (Deutsche Forschungsgemeinschaft, Bonn, Germany). He is currently with the Climate Change Strategies Study at the International Institute for Applied Systems Analysis (IIASA), Laxenburg, Austria.

Michel den Elzen is from the Center for Mathematical Methods, The Netherlands' National Institute of Public Health and Environmental Protection (RIVM), P.O. Box 1, NL–3720 BA Bilthoven, The Netherlands.

Krzysztof Olendrzyński is on leave from the Institute of Meteorology and Water Management (IMWM), Warsaw, Poland. He is currently with the Climate Change Strategies Study at IIASA.

FOREWORD

This paper is the first report of a collaborative effort between IIASA and The Netherlands' National Institute of Public Health and Environmental Protection (RIVM), Bilthoven, on developing an integrated model for assessing, in a time-dependent manner, the socio-economic and ecological effects of a given greenhouse gas scenario. This involves linking greenhouse gas emission accounting frameworks, models for calculating changes with time of greenhouse gas concentrations and climatic change, and ecological changes such as shifts in growing zones for natural vegetation and agricultural crops, and effects on forest growth, water supply and sea level rise. This paper reports on one of the first steps in this linkage: modifying the climate module of RIVM's Integrated Model to Assess the Greenhouse Effect (IMAGE) to provide appropriate temperature and precipitation scenarios for the ecological models. The work follows in the tradition of both institutions in developing science-based tools for policy analysis.

Anton van der Giessen
Leader
Center for Mathematical Methods

Jan Rotmans
Leader, IMAGE Project

Bo R. Döös
Leader
Environment Program

Roderick W. Shaw
Leader, Global Environmental
Security Project

ACKNOWLEDGMENTS

The authors would like to thank J. Rotmans, B.J. de Haan, J. van Eijkeren, and other scientists from The Netherlands' National Institute of Public Health and Environmental Protection (RIVM) for their valuable discussions, comments and encouragement. We would also like to thank R. Shaw from IIASA for his helpful comments and reviewing the manuscript. Finally, we would like to acknowledge the financial support we received through RIVM from the Dutch National Programme on Global Atmospheric Pollution and Climate Change.

TABLE OF CONTENTS

1. SUMMARY 1

2. INTRODUCTION 2

3. METHODOLOGY 4

3.1. Basic Model Equations 4

3.2. Integration into IMAGE 10

3.3. Analytical Solution of the Basic Model 13

3.3.1. Global response 13

3.3.2. Hemispherical responses 15

3.4. Refined Model Equations 20

4. RESULTS 25

4.1. Transient Simulations 26

4.2. Time-Dependent Simulations 27

5. CONCLUSIONS AND OUTLOOK 28

FIGURES 29

APPENDIX 45

REFERENCES 51

A TIME DEPENDENT ZONALLY AVERAGED ENERGY BALANCE MODEL TO BE INCORPORATED INTO IMAGE

(INTEGRATED MODEL TO ASSESS THE GREENHOUSE EFFECT)

Matthias Jonas (IIASA), Michel den Elzen (RIVM), and Krzysztof Olendrzyński (IIASA)

1. SUMMARY

The Intergovernmental Panel on Climate Change (IPCC) is placing increasing emphasis on the use of time-dependent impact models that are linked with energy-emission accounting frameworks and models that predict in a time-dependent fashion important variables such as atmospheric concentrations of greenhouse gases, surface temperature and precipitation. Integrating these tools (greenhouse gas emission strategies, atmospheric processes, ecological impacts) into what is called an *integrated assessment model* will assist policymakers in the IPCC and elsewhere to assess the impacts of a wide variety of emission strategies.

The *Integrated Model to Assess the Greenhouse Effect (IMAGE;* developed at RIVM*)* represents such an integrated assessment model which already calculates historical and future effects of greenhouse gas emissions on global surface temperature, sea level rise and other ecological and socioeconomic impacts.

However, to be linked to environmental impact models such as the Global Vegetation Model and the Timber Assessment Model, both of which are under development at RIVM and IIASA, IMAGE needs to be regionalized in terms of temperature and precipitation output. These key parameters will then enable the above environmental impact models to be run in a time-dependent mode.

In this paper we lay the scientific and numerical basis for a two-dimensional Energy Balance Model (EBM) to be integrated into the climate module of IMAGE which will ultimately provide scenarios of surface temperature and precipitation, resolved with respect to latitude and height. This paper will deal specifically with temperature; following papers will deal with precipitation.

So far, the relatively simple EBM set up in this paper resolves mean annual surface temperatures on a regional scale defined by 10° latitude bands. It belongs to a class of energy balance models (Budyko–Sellers type) which have been widely examined in the literature. Its implementation constitutes what we sometimes term the *first level of modeling.* Although our model is still simple – no distinction is yet made between land, ocean and atmosphere and, also, a deep ocean is not incorporated – its implementation is an important step in the modeling hierarchy. Because of its simplicity we achieve a better understanding, both analytically and numerically, of

how the various parameterizations of the energy fluxes determine the basic behavior of our EBM. In addition, we can concentrate on the implementation of the EBM into IMAGE, i.e., on the steering mechanism itself. Both reasons justify the time and effort put into the first level of modeling.

2. INTRODUCTION

Evidence is mounting that increasing atmospheric concentrations of greenhouse gases (CO_2, CH_4, CO, N_2O, O_3, CFCs, HFCs, and others) are influencing the radiative balance of the earth and bringing about global change. Not only will this global change manifest itself in altered patterns of atmospheric temperature and precipitation, but there could also be a set of associated environmental problems such as rises in sea level, shifts in the growing zones for vegetation (both natural and agricultural), and changes in the supply of freshwater for human use.

The Intergovernmental Panel on Climate Change (IPCC) is placing increasing emphasis on the use of time-dependent impact models that are linked with energy-emission accounting frameworks and models that predict in a time-dependent fashion important variables such as atmospheric concentrations of greenhouse gases, temperature and precipitation. Integrating these tools (greenhouse gas emission strategies, atmospheric processes, ecological impacts) into what is called an *integrated assessment model* will assist policymakers in the IPCC and elsewhere to assess the impacts of a wide variety of emission strategies. To be useful to decisionmakers, an integrated assessment model must have a reasonably quick turnaround time and give results which are in good agreement with Global Circulation Models (GCMs). GCMs, although they are extremely useful as tools for scientific research, are too time-consuming and thus too costly to be very useful for policy analyses. This means that the integrated assessment model should not compete with GCMs but be complementary to them and take advantage of the scientific results from them.

The *Integrated Model to Assess the Greenhouse Effect (IMAGE)* represents such an integrated assessment model which already combines most of the above needs (*cf. Figure 1*). This parameterized science-based simulation policy model has been developed by The Netherlands' National Institute of Public Health and Environmental Protection (RIVM) for the calculation of historical and future effects of greenhouse gas emissions on global surface temperature, sea level rise, and other ecological and socioeconomic impacts (Rotmans 1990). IMAGE is being used by the IPCC and will also soon be used by the EC.

Although the effects of greenhouse gas emissions have been resolved on a hemispherical scale in the meanwhile, there is a need to regionalize IMAGE on a finer regional scale in terms of temperature and precipitation. These two parameters are considered to be key input variables for subsequent regional time-dependent impact studies such as IIASA's Global Vegetation Model (Leemans 1989) which is being further developed by RIVM, and the Timber Assessment Model (Nilsson *et al.* 1991) which has been developed jointly by IIASA's Forestry Study and the Swedish University of Agricultural Sciences. Within the framework of the IMAGE–Project these regional temperature and precipitation projections will be used for socioeconomic impact studies (den Elzen and Rotmans 1991) and for the climate feedback study (den Elzen *et al.* 1991).

It is the objective of this paper to lay the scientific and numerical basis for a two-dimensional Energy Balance Model (EBM; resolving latitude and height) which is to be integrated into the climate module of IMAGE. Its output will ultimately be zonally averaged scenarios of surface temperature and precipitation. The EBM will be steered in a time-dependent mode by the atmospheric concentrations of CO_2 and of the other greenhouse gases, as calculated by the energy-emission accounting framework of IMAGE.

In this paper we constrain ourselves to a class of energy balance models which were first studied by Budyko (1969) and Sellers (1969), and which were further developed and analyzed by Held and Suarez (1974), North (1975a,b), North *et al.* (1978, 1979, 1981), and others. We set up a time-dependent one-dimensional EBM, resolving mean annual surface temperature on a regional scale defined by 10° latitude bands only. Other details such as the separation of land, ocean, sea ice, and atmosphere are still missing. In addition, a global diffusive deep ocean model of IMAGE, which has recently been extended to a two-dimensional advective–diffusive fashion by den Elzen and de Haan (1991), has not yet been incorporated. In particular, the latter entails a sincere shortcoming in light of the fact that the deep ocean has a considerable heat capacity and thus causes the earth to respond to an increase in atmospheric greenhouse gas concentrations on a different time scale, as is well known (IPCC 1990).

However, there are good reasons to start in a simple fashion and to follow a hierarchical development of the EBM. First, there is a need to change the global steering mechanism, which is provided by IMAGE through the atmospheric concentrations of CO_2 and the other greenhouse gases, into a regional one. To accomplish this one has to review the physical importance and the regional distribution of the major effective greenhouse gases. This process of regionalization must happen in parallel to the development of the EBM.

Second, to integrate the EBM into IMAGE in a compatible way, we must ultimately be in the position to understand how the various parameterizations that are used in the EBM to link the energy fluxes to surface temperatures, influence the behavior of the model.

Finally, it is worth recalling that energy balance models are expected to work on time scales that are long compared with those of synoptic weather fluctuations and on spatial scales that are large. For smaller space or time scales, the relatively simple energy balance model will fail because it neglects many physical processes, mean motions, etc., which affect the small-scale structure of the system. On the other hand, by taking averages over large distances and long time periods, one gains the advantage of adding information that is assumed to be statistically uncorrelated and therefore similar to an ensemble average. We wish to take advantage of this admittedly optimistic assumption (North *et al.* 1979) when integrating a regional climatic model into IMAGE. In addition, the basic premise of such modeling is that the large-scale zonally averaged features of the earth's climate can be simulated by parameterizations based solely on empirical functions of the surface temperature. Although much research remains to be done before the extent to which this premise is true can be evaluated, many scientists consider that these low-resolution, highly parameterized models have an important role to play in developing our knowledge of the workings of climate (IPCC 1990).

3. METHODOLOGY

The primary focus of this chapter will be to lay a solid analytical and numerical base for a more advanced EBM. In Section 3.1. we set up an EBM which we call the *basic EBM* and describe the parameterizations of the various energy fluxes. In Section 3.2. we link the basic EBM with IMAGE and explain how it is being steered by IMAGE. In Section 3.3. we develop our basic EBM analytically but, for reasons of mathematical simplicity, for two hemispheres only. However, this procedure provides enough insight in understanding the more highly resolved basic EBM (18 latitude belts of 10° width each). The runs of all model versions are documented in Chapter 4 and compared with IMAGE as a standard, as is the case for the refined EBM. When using the term *refined EBM*, we refer to the basic EBM for which an improved set of parameterizations has been introduced; they are explained in detail in Section 3.4.

3.1. Basic Model Equations

To set up the equations of an EBM, it is necessary to assume that all energy fluxes can be parameterized by the temperature at the earth's surface. Mean annual surface (air) temperatures over both land (ST) and sea (SST) are considered. We have chosen land surface temperatures because a greater variety of parameterizations are available for them. Observed annual mean surface temperatures in the middle of each 10° latitude belt and those obtained by area-weighted, three-point binomial smoothing by latitude are listed for 10° latitude zones in *Table 1.* Both are taken from Warren and Schneider (1979). We use the latter one throughout the whole working paper, when using the terms *surface temperature* or *temperature.*

In the latitude-dependent models of the Budyko–Sellers type it is assumed that the net rate at which heat enters each 10° latitude belt during the year is exactly balanced by the net rate of loss. The individual terms are schematically represented for the i-th latitude belt by

$$(\text{solar in})_i - (\text{infrared out})_i - (\text{net horizontal transport})_i = 0. \tag{1}$$

A common factor, the area of the belt, may be canceled throughout, so that the remaining terms have units of energy per unit time per unit area (watts per square meter).

However, the assumption that there is no net heat flux into the oceans and cryosphere can only be valid when comparing successive years. Because the world ocean has a considerable heat capacity and the global radiation budget is not balanced while the ocean is being heated up (Siegenthaler and Oeschger 1984), we must take a heat storage term into account. Equation (1) then reads

$$(\text{heat stored})_i = (\text{solar in})_i - (\text{infrared out})_i - (\text{net horizontal transport})_i \; . \tag{2}$$

Table 1. Mean annual zonal data of the basic EBM.

Zone	Latitude	f [1]	T_{obs} [2] in °C	T [3] in °C	R [4] in $10^7 \frac{J}{m^2 °C}$	S [5]	a [6]	α_{obs} [7]	IR_{obs} [8] in $\frac{W}{m^2}$	IR [9] in $\frac{W}{m^2}$	NR_{obs} [10] in $\frac{W}{m^2}$	HT [11] in $\frac{W}{m^2}$
1	90–80° N	0.008	−18.0	−16.9	14.53	0.528	2.895	0.589	174.7	179.6	−103.2	−79.3
2	80–70° N	0.023	−12.7	−12.3	10.74	0.571	2.892	0.544	178.2	187.8	−93.6	−67.6
3	70–60° N	0.037	−5.5	−5.1	10.06	0.651	2.864	0.452	189.1	200.6	−72.1	−49.2
4	60–50° N	0.050	2.2	2.2	13.37	0.758	2.885	0.407	201.2	213.6	−46.7	−30.6
5	50–40° N	0.062	8.4	8.8	15.71	0.881	2.895	0.357	218.3	225.4	−20.9	−13.8
6	40–30° N	0.071	15.9	16.2	17.76	1.003	2.857	0.309	239.6	238.5	0.7	5.1
7	30–20° N	0.079	23.2	22.9	19.52	1.111	2.820	0.272	258.5	250.5	18.2	22.2
8	20–10° N	0.084	26.3	26.1	22.45	1.191	2.796	0.248	257.1	256.2	45.5	30.3
9	10– 0° N	0.087	26.3	26.4	23.92	1.233	2.802	0.254	250.0	256.7	58.9	31.1
10	0–10° S	0.087	26.2	26.1	23.62	1.233	2.789	0.241	258.2	256.2	56.1	30.3
11	10–20° S	0.084	24.6	24.6	23.92	1.191	2.784	0.236	266.7	253.5	40.7	26.5
12	20–30° S	0.079	21.4	21.4	23.62	1.111	2.799	0.251	262.7	247.8	22.0	18.4
13	30–40° S	0.071	16.6	16.5	27.43	1.003	2.844	0.296	244.4	239.1	0.4	5.9
14	40–50° S	0.062	9.7	9.9	29.49	0.881	2.905	0.358	224.4	227.3	−27.3	−11.0
15	50–60° S	0.050	2.8	2.9	31.09	0.758	2.910	0.426	206.9	214.9	−57.4	−28.8
16	60–70° S	0.037	−6.0	−6.9	30.74	0.651	2.909	0.513	189.6	197.4	−85.6	−53.8
17	70–80° S	0.023	−33.3	−29.5	16.20	0.571	2.795	0.602	163.3	157.2	−89.5	−111.4
18	80–90° S	0.008	−43.8	−42.3	16.20	0.528	2.695	0.617	154.3	134.4	−87.7	−144.1

Table 1 continued:

1) Normalized area of latitude belt i; *cf. Appendix A.*

2) Observed surface temperatures; taken from Warren and Schneider (1979).

3) Surface temperatures obtained by area-weighted, three-point binomial smoothing of observed data; taken from Warren and Schneider (1979).

4) Effective thermal inertia derived from area-weighting the thermal inertias of land and oceanic mixed layer whereas the thermal inertia of the atmosphere is neglected. Because of its minor importance, we used in each zone the same value for the thermal inertia of land ($0.16 \cdot 2.09\ \mathrm{W\,y\,m^{-2}\,^{\circ}C^{-1}} = 1.05 \cdot 10^7 J\,\mathrm{m^{-2}\,^{\circ}C^{-1}}$ according to North *et al.* 1981). The zonal fractions of land and ocean are from Harvey (1988). The thermal inertias of the mixed layers are derived by the product of mixed layer depth with density ($= 1025\ \mathrm{kg\,m^{-3}}$) and specific heat ($= 3.95 \cdot 10^3\ J\,\mathrm{kg^{-1}\,^{\circ}C^{-1}}$) of seawater. The zonal mixed layer depths are based on Harvey (1988). Following Warren and Schneider (1979) and Harvey (1988), we also assume that oceans in latitudes higher than 70° N and entire zones lower than 70° S are replaced by sea ice with an effective mixed layer depth of 40 m.

5) Weighting function accounting for the latitudinal change in solar radiation; from Eq. (3).

6) From Eq. (7) when tuned against observations.

7) Observed planetary albedo; from Ellis and Vonder Haar (1976).

8) Observed IR flux; from Ellis and Vonder Haar (1976).

9) Calculated IR flux using $A + BT_i$ with $A = 209.7\ \mathrm{W\,m^{-2}}$ and $B = 1.78\ \mathrm{W\,m^{-2}\,^{\circ}C^{-1}}$ from a least-squares fit.

10) Observed net radiation; from Ellis and Vonder Haar (1976).

11) Calculated net horizontal energy transport using $\gamma(T_i - T_o)$ with $\gamma = 2.55\ \mathrm{W\,m^{-2}\,^{\circ}C^{-1}}$ from a least-squares fit.

Each of these terms can be parameterized by some theoretical or semi-empirical formula in terms of today's surface temperature field. The change in latitudinal heat storage is expressed by $R_i \frac{dT_i(t)}{dt}$ where R_i is the effective heat capacity of the relevant layers of the atmosphere plus hydrosphere (oceanic mixed layer only) per m^2 of earth surface (*cf. Table 1*). This quantity is usually termed *thermal inertia* in literature. T_i is the surface temperature in latitude belt i. We have not yet assumed R_i to depend on temperature. Some simple calculations indicate that this assumption deserves further attention.

The incoming solar flux in Eq. (2) is given at the top of the atmosphere by $Q_0 S_i(1-\alpha_i(t))$. Q_0 is the solar constant divided by 4 and assumed constant for our purposes. It is well to note that the value of the solar constant for the basic model ($1364\ W\,m^{-2}$; Sections 3.1. to 3.3.) is different from that for the refined model ($1340\ W\,m^{-2}$; Section 3.4.). This is a consequence of forcing the models' unperturbed climate to fit the present climate. North *et al.* (1981) give a justification for this process referred to as *tuning*. The value from the Nimbus 7 satellite measurements is $1376\ W\,m^{-2}$.

S_i is determined by $S(x)$, the (normalized) mean annual meridional distribution of the solar radiation, which is approximated from astronomical calculations by

$$S(x) \cong 1 + S_2 P_2(x) \tag{3}$$

with $S_2 = -0.477$, $x = \sin\theta$, θ being the latitude and $P_2(x)$ the second Legendre polynomial, $P_2(x) = \frac{1}{2}(3x^2 - 1)$ (North *et al.* 1981). Note that $\sin\theta$ is a convenient variable to use in zonal average applications because dx is proportional to the area of a latitude strip; i.e., in the case of $S(x)$:

$$\frac{1}{2}\int_{-1}^{1} S(x)\,dx = \int_{0}^{1} S(x)\,dx = 1 \tag{4}$$

or in the discrete case of S_i:

$$\sum_{i=1}^{n} f_i S_i = 1 \tag{5}$$

where $n\,(=18)$ is the amount of latitudinal zones and

$$\sum_{i=1}^{n} f_i = 1 \tag{6}$$

(*cf. Appendix A*). The weighting terms accounting for the latitudinal fraction of both mean annual solar radiation and area, S_i and f_i, respectively, are listed in *Table 1*.

For obvious reasons, the albedo α_i is expressed as a function of time when temperature is assumed to depend on time. A standard argument is that a changing climate entails a changing ice line which, in turn, has a major influence on the albedo. To start with we shall use Sellers' (1969) zonal albedo parameterization:

$$\alpha_i(t) = \alpha_i(T_i(t)) = \begin{cases} a_i + b(273.15 + T_i(t)) & T_i(t) \leq 10^\circ\mathrm{C} \\ \text{for} & \\ a_i + b(273.15 + 10) & T_i(t) > 10^\circ\mathrm{C} \end{cases} \tag{7}$$

This relation with temperature is made plausible by North and Coakley (1979) (*cf.* also ***Figure 2***). In this formulation, the albedo is a function of temperature only when the mean annual zonal temperature is low enough ($\leq 10^\circ$C) to expect snow or sea-ice cover for at least part of the year at some longitudes within the zone. Because of the nonuniform land–sea distribution, the snow line does not follow a latitude line. Sellers' formula accounts for this by allowing the zonal albedo to vary smoothly, rather than abruptly, with latitude. For any given value of b, the temperature-independent parameters a_i are tuned to give the present observed mean annual values of zonal planetary albedo; both are listed in *Table 1*. The parameter b is the ***albedo-temperature feedback coefficient*** which Sellers thought most likely to be uniformly $-0.009^\circ\mathrm{C}^{-1}$ (Warren and Schneider 1979). We discuss the shortcomings of this parameterization and proceed with improvements in Section 3.4.

The outgoing infrared flux in Eq. (2) is, strictly speaking, proportional to the fourth power of the characteristic radiating temperature of the earth according to the Stefan–Boltzmann law, but over the small temperature range of interest on the absolute scale this relationship can be considered linear (Henderson–Sellers and McGuffie 1987). Moreover, the IR flux at the top of the atmosphere is even related to surface temperature by $A(t) + BT_i(t)$. $A(t)$ and B are empirical parameters designed to account for the greenhouse effect of clouds, water vapor, CO_2, CH_4, CFCs, N_2O, and other greenhouse gases. It is a standard practice to lump the effect of increasing CO_2 (or CO_2–equivalent) concentration into the coefficient A following Ramanathan *et al.* (1979). A decrease in A is thought to mimic the radiative effect of an increase in CO_2 but there is no obvious reason why B should not change. However, for reasons of simplicity, we adopt this procedure in our paper as well. For today's climate represented by surface temperatures $A = 209.7\ \mathrm{W\,m^{-2}}$ and $B = 1.78\ \mathrm{W\,m^{-2}\,^\circ C^{-1}}$ are derived by a least-squares fit against observations from Ellis and Vonder Haar (1976) (*cf. Table 1* and ***Figure 9***). Values of $A(t)$ for changing climates are calculated by IMAGE (*cf.* Section 3.2.). Improvements of this IR parameterization are discussed in Section 3.4.

The term for the net horizontal energy transport in Eq. (2) is also a linear function of surface temperature, $\gamma(T_i(t) - T_0(t))$, where $T_0(t)$ is defined to be the global average of surface temperature,

$$T_0(t) = \sum_{i=1}^{n} f_i T_i(t) \tag{8}$$

(= 14.23° C for today's surface temperatures listed in *Table 1*).

This parameterization was suggested by Budyko (1969) and is a fit to observed temperatures and to calculated net radiation, and is not meant to model any individual physical transport process. This was the reason why Warren and Schneider (1979) expressed their limited confidence that this formula would be reliable for predicting the net heat transport of a changed climate. However, North *et al.* (1981) showed that

a net diffusive heat transport with constant diffusion coefficient, when temperature is approximated by Legendre polynomials and truncated after the second mode, results in a linear expression which is equivalent to Budyko's. For that reason, we assume that the above parameterization serves our initial purpose of being useful within a simple EBM.

The subsequent definition for $T_0(t)$ (Eq.(8)) must be thought of as a consequence of the initial assumption that all energy fluxes can be parameterized by the surface temperature. From the point of view of thermodynamics, one should keep in mind that the mean temperature is derived from a weighted sum in which the weighting is given by heat capacities and not by the area of the latitude belts.

When fitting the net horizontal energy transport to observations by least-squares we find the parameter $\gamma = 2.55\ \mathrm{W\,m^{-2}\,^{\circ}C^{-1}}$ compared to $3.74\ \mathrm{W\,m^{-2}\,^{\circ}C^{-1}}$ of Budyko who considered the northern hemisphere only (*cf. Table 1* and *Figure 4*). We are aware that this low value increases the global stability of our model which was defined by Lindzen and Farrell (1977) as the ability of the earth to resist total glaciation in the face of a large reduction in solar luminosity. The discussion on this matter is resumed in Section 3.4.

Inserting the various parameterizations discussed, Eq. (2) can now be summarized by

$$R_i \frac{dT_i(t)}{dt} = Q_0 S_i(1-\alpha_i(t)) - (A(t)+BT_i(t)) - \gamma(T_i(t)-T_0(t)) \ , \tag{9}$$

together with the already introduced equations

$$\alpha_i(t) = \alpha_i(T_i(t)) = \begin{cases} a_i + b(273.15+T_i(t)) & T_i(t) \le 10^{\circ}\mathrm{C} \\ \text{for} & \\ a_i + b(273.15+10) & T_i(t) > 10^{\circ}\mathrm{C} \end{cases} \tag{7}$$

and

$$T_0(t) = \sum_{i=1}^{n} f_i T_i(t) \ . \tag{8}$$

This is the basic set of equations which will be further developed and used in the following section. The goal will be to integrate these equations into the climate module of IMAGE and make use of the current steering mechanism of IMAGE as given by the radiative forcing.

3.2. Integration into IMAGE

Equations (7),(8),(9) can alternatively be expressed in terms of a change in zonal surface temperature, $\Delta T_i(t) = T_i(t) - T_i(t=0)$:

$$R_i \frac{d\Delta T_i(t)}{dt} - R_i \frac{dT_i(t)}{dt}\bigg|_{t=0} = -Q_0 S_i \Delta\alpha_i(t) - (\Delta A(t) + B\Delta T_i(t)) \qquad (10)$$

$$-\gamma(\Delta T_i(t) - \Delta T_0(t)) \ ,$$

$$\Delta\alpha_i(t) = \alpha_i(t) - \alpha_i(t=0) = \begin{cases} b\Delta T_i(t) & T_i(t)\ ,\ T_i(t=0) \le 10°C \\ b(10 - T_i(t=0)) \ \text{for} & T_i(t) > 10°C\ ,\ T_i(t=0) \le 10°C \\ 0 & T_i(t)\ ,\ T_i(t=0) > 10°C \end{cases} \qquad (11)$$

where it is assumed that $T_i(t) \ge T_i(t=0)$, and

$$\Delta T_0(t) = \sum_{i=1}^{n} f_i \Delta T_i(t) \ , \qquad (12)$$

where $\Delta A(t)$ stands for the difference $A(t) - A(t=0)$ and $t = 0$ refers to preindustrial conditions (here taken to be in 1900). For this time the second term on the left side of Eq. (10) equilibrium is supposed to be zero.

Globally averaging Eq. (10) yields

$$R_0 \frac{d\Delta T_0(t)}{dt} = -Q_0 \Delta\alpha_0(t) - (\Delta A(t) + B\Delta T_0(t)) \ . \qquad (13)$$

Here we made use of

$$R_0 \frac{dT_0(t)}{dt} = \sum_{i=1}^{n} f_i R_i \frac{dT_i(t)}{dt} \ , \qquad (14)$$

the change in global heat storage, and

$$\alpha_0(t) = \sum_{i=1}^{n} f_i S_i \alpha_i(t) \ , \qquad (15)$$

the definition for the global albedo (*cf. Appendix B*). If also expressed in terms of temperature changes, both equations read:

$$R_0 \frac{d\Delta T_0(t)}{dt} = \sum_{i=1}^{n} f_i R_i \frac{d\Delta T_i(t)}{dt} \ , \qquad (16)$$

$$\Delta\alpha_0(t) = \sum_{i=1}^{n} f_i S_i \Delta\alpha_i(t) \ . \qquad (17)$$

The climate module of IMAGE incorporates a global energy balance model which is coupled to an advective–diffusive deep ocean model and is based on Wigley and Schlesinger (1985) and Wigley and Raper (1987). This climate model includes a land box, a deep ocean and an ocean mixed layer box, and atmosphere boxes over land and ocean. The basic model equations are described in Rotmans (1990), and den Elzen and de Haan (1991). The hemispherical surface temperature changes over both land and ocean are calculated just as the oceanic temperature changes with depth.

Since we do not yet distinguish between land and ocean, and assume a zero net heat flux into the deep ocean, we must somewhat simplify the equation used by IMAGE to the equation given by Dickinson (1986):

$$R_0 \frac{d\Delta T_0(t)}{dt} = \Delta Q(t) - \lambda_0 \Delta T_0(t) \quad . \tag{18}$$

Here $\Delta Q(t)$ (in $\mathrm{W\,m^{-2}}$) is the net change in the solar plus terrestrial radiation at the top of the atmosphere due to the change of some external parameter, assuming present climate. Parameters that are regarded as not controlled by the climate system (such as the solar luminosity and the anthropogenic influence on greenhouse gas concentrations in the atmosphere) are referred to as external parameters by Dickinson. $\Delta Q(t)$ is usually termed *total radiative forcing.* By taking the system's ability of storing heat into account, the term $\lambda_0 \Delta T_0(t)$ approximates the net change of the vertical radiative energy flux at the top of the atmosphere, resulting from a global temperature change. It describes how the climate system (represented by $T_0(t)$) changes in response to a given radiative forcing $\Delta Q(t)$. The factor λ_0 (in $\mathrm{W\,m^{-2}\,^{\circ}C^{-1}}$) is referred to as the *global feedback parameter.* It includes all the feedbacks (positive and negative) that act to displace or restore temperature from or to its equilibrium value in the absence of $\Delta Q(t)$.

Comparing Eqs. (18) and (13), we find

$$\Delta Q(t) = -\Delta A(t) \tag{19}$$

and

$$\lambda_0 \Delta T_0(t) = Q_0 \Delta \alpha_0(t) + B \Delta T_0(t) \tag{20}$$

where we do not yet specify how to parameterize $\Delta\alpha_0(t)$ in terms of $\Delta T_0(t)$. This is because of the inapplicability of the temperature conditions in Eq. (7) or (11) when used globally: if we assume a reduction of the number of latitudinal zones (upper index limit, n, decreasing), the corresponding zonal surface temperatures approach each other. Those of the lower latitudes take on smaller temperature values, those of the higher latitudes greater values. Finally, we consider the whole sphere as one zone ($n = 0$). Since the corresponding global surface temperature is greater than 10°C (the today's value is 14.23°C), the last temperature condition in Eq. (11) would imply that the global albedo would not change any more in case of a temperature change. This would be the more surprising because today's ice line is located at about $x_{\mathrm{ice}} = 0.95$ ($\theta \approx 72^{\circ}$) which leaves, in case of a temperature change, no doubt about a change in global albedo. However, Eq. (20) already gives us a first insight into the global feedback parameter λ_0.

Equation (19) states that the change in the IR parameter $A(t)$ is given by the total radiative forcing, $\Delta Q(t)$. This quantity, in turn, is calculated by IMAGE from the concentration of CO_2–equivalent in the atmosphere according to

$$\Delta Q(t) = \frac{\Delta Q_{2\times CO_2}}{ln2} \cdot \ln\left[\frac{pCO_{2,eq}(t)}{pCO_2(t=0)}\right] \tag{21}$$

(Rotmans 1990). Here

$\Delta Q_{2\times CO_2}$ = radiative forcing for a doubled atmospheric CO_2 concentration; the value used in IMAGE is $4.32\ W\,m^{-2}$ in accordance with the IPCC (1990).

$pCO_{2,eq}(t)$ = atmospheric CO_2–equivalent concentration (in ppm).

$pCO_2(t=0)$ = preindustrial (i.e., 1900) atmospheric CO_2 concentration (in ppm).

Following concluding remarks must be added:

(1) Equation (18) separates the calculation of a global temperature change into two distinct questions (Dickinson 1982). First, what is the change of the global heat balance due to the change of some external parameter assuming present climate ($\Delta Q(t)$)? Second, taking the system's ability of storing heat into account, how does the climate system change ($\lambda_0 \Delta T_0(t)$) in response to a given $\Delta Q(t)$? This thinking implies that the climate change always depends on effects of an external change that can directly be translated into a radiative forcing, i.e., which can be expressed in $W\,m^{-2}$.

(2) The climate change depends in part on the spatial distribution of the $\Delta Q(t)$, e.g., how much $\Delta Q(t)$ is added to the atmosphere versus to the ground and how $\Delta Q(t)$ varies with latitude. Note that the latter case is readily included in Eq. (19) when expressed by area-weighted sums on both sides with respect to $\Delta Q_i(t)$ and $-\Delta A_i(t)$, respectively.

(3) For the present level of modeling, $\Delta Q(t)$ as provided by IMAGE through Eq. (21) will be used. However, the EBM of the next higher level of modeling should make direct use of the atmospheric CO_2–equivalent concentration rather than the total radiative forcing derived therefrom (de Haan 1991). This is because direct-effect $\Delta Q - pCO_{2,eq}$ relationships are calculated using detailed radiative transfer models. Such calculations simulate the complex variations of absorption and emission with wavelength for the various gases, and account for the overlap between absorption bands of the gases; the effects of clouds on the transfer of radiation are also accounted for (IPCC 1990). Therefore, it seems that allowances are made for some effects twice: on the one hand, in radiative transfer models and, on the other hand, in the EBM to be developed.

3.3. Analytical Solution of the Basic Model

In this section we will focus on the global and the hemispherical model responses with respect to both the equilibrium and the transient simulation because of the basic model characteristics they disclose. Both terms in the present context are in accordance with the IPCC (1990). Climate is in *equilibrium* when it is in balance with the radiative forcing (no storage of heat). Most equilibrium experiments consider the effect of doubling the concentration of atmospheric CO_2, since the effect of increases in other trace gases can be calculated in terms of an increase in effective CO_2. Only the radiative effects of increases in greenhouse gases are taken into account. The term *transient simulation* refers to a simulation for which CO_2 is doubled instantaneously and for which the model is then run for some time period to document the climate changes (effective heat storage); if possible, the run is pursued until the new equilibrium is reached.

3.3.1. Global response

Equation (13) with constant albedo ($\lambda_0 = B$ according to Eq. (20)) is the basic equation to be studied in the following. For convenience, we list the parameters used in this subsection:

$-\Delta A(2\times CO_2) = 4.32 \ \mathrm{W\,m^{-2}}$

$A(\text{present}) = 209.7 \ \mathrm{W\,m^{-2}}$

$\lambda_0 = B = 1.78 \ \mathrm{W\,m^{-2}\,^\circ C^{-1}}$

$\lambda_0(\text{IMAGE}) = 1.728 \ \mathrm{W\,m^{-2}\,^\circ C^{-1}}$

$R_0 = 6.84 \ \mathrm{W\,y\,m^{-2}\,^\circ C^{-1}}$ (this is a global mean derived from the hemispherical thermal inertias used in Subsection 3.3.2.).

For the equilibrium simulation the heat storage term on the left side of Eq. (13) is zero thus yielding an increase of the global equilibrium temperature by

$$\Delta T_0(2\times CO_2) = \frac{-\Delta A(2\times CO_2)}{B} = 2.43^\circ C \ . \qquad (22)$$

Note that λ_0 as used in IMAGE yields $\Delta T_0(2\times CO_2) = 2.50^\circ C$ (Eq. (18)). However, we rather judge this close agreement as somewhat fortuitous especially since we do not account for a change in global albedo and, also, the IR parameter B is not known to better than 20% accuracy (Thompson and Warren 1982).

An important parameter in this context is the *equilibrium global sensitivity parameter* β_0 (North *et al.* 1981, Schneider and Thompson 1981), here taken with respect to an anthropogenic CO_2–equivalent increase

$$\beta_0 = \frac{A}{100}\frac{\partial T_0}{\partial A} \quad . \tag{23}$$

The parameter β_0 is a measure of the change in global surface temperature due to a 1% change in the IR parameter A. For all climate models, β_0 is the first quantity to compute because the sensitivity of the model to any perturbation is roughly proportional to β_0.

Expressing Eq. (13) in terms of $T_0(t)$ rather than $\Delta T_0(t)$, solving for $T_0(t)$ and inserting into Eq. (23), we find

$$\beta_0(\text{present}) = -\frac{A(\text{present})}{100B} = 1.18^\circ\text{C} \quad . \tag{24}$$

The minus sign comes in because a decrease in $A(t)$ is related to an increase in $T_0(t)$ and vice versa.

For the transient simulation we retain the heat storage term on the left side of Eq. (13). For reasons of convenience, we consider an instantaneous decrease in radiative forcing at $t = 0$, say from $\Delta Q(2 \times CO_2)$, to zero first. We then have to solve

$$D\Delta T_0(t) + \frac{B}{R_0}\Delta T_0(t) = 0 \tag{25}$$

with D as an abbreviation for the differential operation $\frac{d}{dt}$. The solution is given by

$$\Delta T_0(t) = ce^{-\frac{B}{R_0}t} = 2.43 \cdot e^{-0.260\frac{1}{y}t}\,^\circ\text{C} \tag{26}$$

where the constant c satisfies the initial condition $\Delta T_0(t=0) = 2.43^\circ\text{C}$. However, in case of a temperature increase following an instantaneous doubling of CO_2, we rather have to adjust Eq. (26) to the initial condition $\Delta T_0(t=0) = 0^\circ\text{C}$ which can be accomplished by

$$\Delta T_0(t) = 2.43\left[1 - e^{-0.260\frac{1}{y}t}\right]^\circ\text{C} \quad . \tag{27}$$

Equation (27) describes how the global system (represented by $T_0(t)$) is approaching the new equilibrium of $2 \times CO_2$ as a consequence of an effective global thermal inertia. The speed of the temperature response and the influence of the thermal inertia can be characterized by the *e-folding* time, τ_0, defined by $\Delta T(\tau_0) = \Delta T(2 \times CO_2)(1 - e^{-1})$. For the global system discussed above, $\tau_0 = \frac{R_0}{B}$ is in the order of 3.84 y.

3.3.2. Hemispherical responses

We will gain further insight into the more complex behavior of our system if we subdivide the earth into regions. In order to keep the analytical solution manageable, we have to constrain ourselves to a hemispherical subsystem. Equations (10),(11),(12) for $i = 1$ (NH, northern hemisphere), 2 (SH, southern hemisphere) are now the basic equations to be studied with respect to the equilibrium and the transient simulations. Again, we will not consider a change in the hemispherical albedos (today's temperature values of the northern and southern hemisphere are 15.03°C and 13.44°C, respectively). However, we will make it clear how the albedo changes will come into the general solutions of the hemispherical temperature responses.

The parameters to be used in this subsection are

$$f_1 = f_2 = \frac{1}{2} \text{ (according to Eq. (6))}$$

$$S_1 = S_2 = 1 \text{ (from Eq. (5))}$$

$$-\Delta A(2\times CO_2) = 4.32 \text{ W m}^{-2}$$

$$B = 1.78 \text{ W m}^{-2}\,^{\circ}\text{C}^{-1}$$

$$\gamma = 2.55 \text{ W m}^{-2}\,^{\circ}\text{C}^{-1}$$

$$R_1 = 5.78 \text{ W y m}^{-2}\,^{\circ}\text{C}^{-1}$$

$$R_2 = 7.90 \text{ W y m}^{-2}\,^{\circ}\text{C}^{-1}$$

The hemispherical thermal inertias are estimated to a first order from

$$R_i = \frac{\rho_{sw} \cdot h_{ml} \cdot F_i \cdot f_{o,i} \cdot c_{sw}}{F_i} \tag{28}$$

where

ρ_{sw} = density of seawater (1025 kg m^{-3}; *cf.* Table 1-46 in Bolz and Tuve 1973)

h = depth of mixed layer (75 m)

F_i = area of hemisphere

$f_{o,i}$ = fraction of hemisphere i covered by ocean; $f_{o,1} = 0.60$, $f_{o,2} = 0.82$ (calculated from Table 1 in Harvey 1988)

c_{sw} = specific heat capacity of seawater (3.95 kJ kg^{-1}°C^{-1}; *cf.* Table 1-46 in Bolz and Tuve 1973).

The global thermal inertia can then be derived from

$$R_0 = \sum_{i=1}^{2} f_i R_i = 6.84 \frac{\text{W y}}{\text{m}^2\,^{\circ}\text{C}} \quad . \tag{29}$$

This is the value used in Section 3.3.1.

For the equilibrium simulation we have to insert Eqs. (11) (first and third temperature case) and (12) into Eq. (10) where Eq. (12) is expressed with respect to another summation index (j). After re-arranging terms, we find

$$\Delta T_i - \frac{\gamma}{\lambda_i} \sum_{j=1}^{n} f_j \Delta T_j = \frac{-\Delta A}{\lambda_i} \tag{30}$$

with

$$\lambda_i = \begin{cases} Q_0 b S_i + B + \gamma & \text{for } T_i(t)\ ,\ T_i(t=0) \le 10^\circ\text{C} \\ B + \gamma & \text{for } T_i(t)\ ,\ T_i(t=0) > 10^\circ\text{C} \end{cases} \tag{31}$$

as the ***latitudinal feedback parameter***. The second temperature condition of Eq. (11) results in $R_i = B + \gamma$ and in an equation similar to Eq. (30) but with the additional constant forcing - $Q_0 b S_i (10 - T_i(t=0)) \ / \ \lambda_i$ on its right side. We do not consider this temperature case in the following.

Eq. (30) can be written more conveniently in the form of a matrix where we already account for $n = 2$ (northern and southern hemisphere)

ΔT_1	ΔT_2	
$1 - \frac{\gamma f_1}{\lambda_1}$	$-\frac{\gamma f_2}{\lambda_1}$	$\frac{-\Delta A}{\lambda_1}$ (32a)
$-\frac{\gamma f_1}{\lambda_2}$	$1 - \frac{\gamma f_2}{\lambda_2}$	$\frac{-\Delta A}{\lambda_2}$. (32b)

Note that the net horizontal heat transport can also be modeled in the form of a thermal diffusion with D as a phenomenological macroturbulent diffusion constant

$$-D\nabla^2 T(x) = -D\frac{d}{dx}\left[(1-x^2)\frac{dT(x)}{dx}\right] \tag{33}$$

(North *et al.* 1981). In this case, many of the matrix elements in the quadratic matrices following (32) (i.e., matrices with $n > 2$) are zero, depending in detail on the difference scheme used for the approximation of the Laplace operator ∇^2.

The solution for the changes in hemispherical equilibrium temperatures can be found by diagonalizing the matrix equations (32a) and (32b). We find for

$$\Delta T_1(2\times CO_2) = \frac{-\Delta A(2\times CO_2)}{\lambda_1 - \gamma} = \frac{-\Delta A(2\times CO_2)}{B} = 2.43^\circ\text{C} \tag{34a}$$

$$\Delta T_2(2\times CO_2) = \frac{-\Delta A(2\times CO_2)}{\lambda_1 - \gamma} = \frac{-\Delta A(2\times CO_2)}{B} = 2.43^\circ\text{C} \tag{34b}$$

(*cf. Appendix C*), i.e., the same value as in the global case. The reason why both hemispheres reveal the same temperature changes after a CO_2 doubling which, in turn, implies no change in the net heat transport is first because no change in albedo has been taken into account and, second, because of our present lack of knowledge with respect to $-\Delta A(2\times CO_2)$ on a smaller scale than global.

It should be mentioned that we have not introduced the equilibrium sensitivity parameter for hemispheres (or even latitudes) which can be defined in an analogous manner as in Eq. (23). This can be made up for as soon as more knowledge on latitudinal A values has been compiled. Ramanathan *et al.* (1979), and Warren and Schneider (1979) have made first attempts in that respect.

For the transient simulation we also have to insert Eqs. (11) (first and third temperature case) and (12) into Eq. (10) and proceed with the resulting equation as done in Section 3.3.1. After re-arranging terms, we find

$$D\Delta T_i(t) = -\frac{\lambda_i}{R_i}\Delta T_i(t) + \frac{\gamma}{R_i}\sum_{j=1}^{n} f_j \Delta T_j(t) \tag{35}$$

with

$$\lambda_i = \begin{cases} Q_0 b S_i + B + \gamma & \\ & \text{for} \\ B + \gamma & \end{cases} \quad \begin{array}{l} T_i(t)\ ,\ T_i(t=0) \le 10^\circ\mathrm{C} \\ \\ T_i(t)\ ,\ T_i(t=0) > 10^\circ\mathrm{C}\ . \end{array} \tag{36}$$

The second temperature condition of Eq. (11) again results in $R_i = B+\gamma$ and in the additional term - $Q_0 b S_i(10 - T_i(t=0))\ /\ R_i$ on the right side of Eq. (35) which is then no longer a homogeneous differential equation. This additional term can be explained as a forcing implied by Sellers temperature restriction on albedo in Eq. (7). Here, again we limit our discussion to Eqs. (35) and (36) in the following.

If we introduce

$$a_{ij} = \begin{cases} \dfrac{\gamma f_j}{R_i} & \\ & \text{for} \\ -\dfrac{\lambda_i - \gamma f_i}{R_i} & \end{cases} \quad \begin{array}{l} i \neq j \\ \\ i = j\ , \end{array} \tag{37}$$

Eq. (35) can be written in the form of a matrix equation where we already account for $n = 2$:

$$\begin{bmatrix} D\Delta T_1(t) \\ D\Delta T_2(t) \end{bmatrix} = \begin{bmatrix} a_{11} & a_{12} \\ a_{21} & a_{22} \end{bmatrix} \begin{bmatrix} \Delta T_1(t) \\ \Delta T_2(t) \end{bmatrix} \tag{38}$$

or

$$D\vec{\Delta T}(t) = M_2\vec{\Delta T}(t) \tag{39}$$

with $M_2 = (a_{ij})$.

In order to solve Eq. (38) or (39) we have to assume a finite net horizontal heat transport ($0 < \gamma < \infty$). Any solution is given by

$$\Delta T(t) = \sum_{k=1}^{2} c_k \vec{h}_k e^{\alpha_k t} \tag{40}$$

where c_1, c_2 are constants, α_1, α_2 the (mutually distinct) eigenvalues of M_2 and $\vec{h}_1$, $\vec{h}_2$ the corresponding eigenvectors (Pontryagin 1962). Note that the indices 1 and 2 of c_k, $\vec{h}_k$, α_k do not follow the hemispherical index breakdown.

The eigenvalues of M_2 are given by

$$\alpha_1 = C + \sqrt{C^2 - D} \tag{41a}$$

$$\alpha_2 = C - \sqrt{C^2 - D} \tag{41b}$$

with

$$C = \frac{a_{11} + a_{22}}{2} \quad , \qquad D = a_{11}a_{22} - a_{12}a_{21} \tag{42), (43}$$

(*cf. Appendix D*) and the corresponding eigenvectors by

$$\vec{h}_1{}^T = (h_{11}, h_{12}) = \left(1, \frac{\alpha_1 - a_{11}}{a_{12}}\right) \tag{44a}$$

$$\vec{h}_2{}^T = (h_{21}, h_{22}) = \left(1, \frac{\alpha_2 - a_{11}}{a_{12}}\right) \tag{44b}$$

(*cf. Appendix E*). Taking the initial conditions $\Delta T_1(t=0) = \Delta T_2(t=0) = 0°\,\mathrm{C}$ into account, we find for the hemispherical temperature changes

$$\Delta T_1(t) = 2.43°\,\mathrm{C} - \left(c_1 e^{\alpha_1 t} + c_2 e^{\alpha_2 t}\right)$$

$$= 2.43°\,\mathrm{C} - \left(2.11 \cdot e^{-0.256\frac{1}{y}t} + 0.31 \cdot e^{-0.659\frac{1}{y}t}\right)°\,\mathrm{C} \tag{45a}$$

$$\Delta T_2(t) = 2.43°\,\mathrm{C} - \left(c_1 \frac{\alpha_1 - a_{11}}{a_{12}} e^{\alpha_1 t} + c_2 \frac{\alpha_2 - a_{11}}{a_{12}} e^{\alpha_2 t}\right)$$

$$= 2.43^{\circ}\mathrm{C} - \left[2.61 \cdot e^{-0.256\frac{1}{y}t} - 0.19 \cdot e^{-0.659\frac{1}{y}t}\right]^{\circ}\mathrm{C} \qquad (45b)$$

(*cf. Appendix F*) from which we can derive with the help of Eq. (12) the globally averaged transient temperature change

$$\Delta T_0(t) = \frac{1}{2}\Delta T_1(t) + \frac{1}{2}\Delta T_2(t)$$

$$= 2.43^{\circ}\mathrm{C} - \left[\frac{1}{2}c_1\left(1+\frac{\alpha_1 - a_{11}}{a_{12}}\right)e^{\alpha_1 t} + \frac{1}{2}c_2\left(1+\frac{\alpha_2 - a_{11}}{a_{12}}\right)e^{\alpha_2 t}\right]$$

$$= 2.43^{\circ}\mathrm{C} - \left[2.36 \cdot e^{-0.256\frac{1}{y}t} + 0.06 \cdot e^{-0.659\frac{1}{y}t}\right]^{\circ}\mathrm{C}\ . \qquad (46)$$

So far, we have to note that the hemispherical breakdown of our system implies a breakdown of our global transient temperature change (Eq. (27)) into two temperature relaxation processes ($e^{\alpha_1 t} = e^{-0.256\frac{1}{y}t}$ and $e^{\alpha_2 t} = e^{-0.659\frac{1}{y}t}$ with e–folding times $\tau_1 = 3.91\,\mathrm{y}$ and $\tau_2 = 1.52\,\mathrm{y}$, respectively) in the hemispherical transient temperature responses (Eqs. (45a), (45b)) and also in the corresponding globally averaged temperature response (Eq. (46)). The two hemispheres differ only with respect to their thermal inertia (because of the different fractions of land and ocean); this is the reason that the two hemispheres approach the new equilibrium of $2 \times CO_2$ in different ways. All the other parameters which could also have some influence on the transient temperature responses themselves or the equilibria to be approached, are the same in both hemispheres (*cf.* λ_i in Eq. (36) and $-\Delta A(2 \times CO_2)$ in Eqs. (34a), (34b)).

The curves of the hemispherical transient temperature changes are depicted and further discussed in the next chapter together with other results (*cf.* Section 4.1.). Here we only like to add two concluding remarks.

(1) The two relaxation processes involved in the hemispherical transient solutions are acting on different time scales. By comparing our temperature responses with those of North *et al.* (1981), we get the indication that the relaxation process with the greater e–folding time ($e^{\alpha_1 t}$) refers to the temperature response of the whole earth while the relaxation process with the smaller e–folding time ($e^{\alpha_2 t}$) refers to the temperature responses on the hemispherical scale (*cf. Appendix G*). Thus, when subdividing the earth latitudinally, we must always keep in mind that this regionalization process implies temperature responses on a finer and finer scale, and that there is a certain limit of resolution we should not exceed with this type of model.

(2) For a zero net horizontal heat transport ($\gamma = 0$) the hemispherical transient temperature responses are given by

$$\Delta T_1(t) = 2.43\left[1 - e^{-\frac{B}{R_1}t}\right]^{\circ}\mathrm{C}$$

$$= 2.43\left[1 - e^{-0.308\frac{1}{V}t}\right]^{\circ}\mathrm{C} \tag{47a}$$

$$\Delta T_2(t) = 2.43\left[1 - e^{-\frac{B}{R_2}t}\right]^{\circ}\mathrm{C}$$

$$= 2.43\left[1 - e^{-0.225\frac{1}{V}t}\right]^{\circ}\mathrm{C} \tag{47b}$$

representing two mutually isolated hemispheres, and for an infinite net transport ($\gamma = \infty$) the temperature responses are given by

$$\Delta T_0(t) = \Delta T_1(t) = \Delta T_2(t) \tag{48}$$

representing an isothermal earth which responds instantaneously to any disturbance in the radiative equilibrium because no relaxation processes are involved. Both extreme cases can be readily derived from Eq. (10).

3.4. Refined Model Equations

In this section, we focus on refining the parameterizations employed for the basic model (Section 3.1.), namely, the parameterizations of the albedo, the outgoing IR flux and the net horizontal energy transport, because they reveal various shortcomings. In the refined EBM we try to overcome some of them. However, we have to keep in mind that it is the degree of the model's spatial resolution in the first instance which sets natural bounds to the various refinements. In order to minimize the use of indices in this section, we will use $x = \sin\theta$ as the independent variable to express the dependence on latitude of the equations to be set up.

(a) Albedo

We begin with the ice-albedo parameterization employed by Sellers (1969). He arrived at the value $b = -0.009^{\circ}\mathrm{C}^{-1}$ by comparing observed zonal albedos and temperatures at similar latitudes in the northern and southern hemisphere. But as pointed out by Gal-Chen and Schneider (1976), the climatology of the two hemispheres differs. In particular, there are differences in cloud amount between the two hemispheres which should introduce a spurious effect into such a zonal albedo comparison. Furthermore, Lian and Cess (1977) argued that the albedo for the ice-covered portion of the hemisphere is greater relative to that of the ice-free portion, not only because of the ice cover, but also as a consequence of the albedo being dependent upon solar zenith angle. In particular, the albedo of clouds is greatly enhanced at high latitudes by this effect. They showed that the neglect of zenith angle dependence leads to an overestimate of the ice-albedo feedback in the Budyko–Sellers type of models.

For these reasons, we decided to follow Lian and Cess' albedo parameterization which accounts for zenith angle effects as well as the influence of latitudinal variations in cloud amount. They employed the latitudinal variation of zonal albedo to determine the dependence of zonal albedo upon surface temperature:

$$\frac{\partial \alpha}{\partial T} = A_c(x) \frac{\partial \alpha_c}{\partial T} + [1 - A_c(x)] \frac{\partial \alpha_s}{\partial T} \tag{49}$$

where α, α_c and α_s denote the zonal effective albedo, the cloudy-sky albedo and the clear-sky albedo, while $A_c(x)$ represents the zonal cloud fraction taken to be constant here (*cf. Table 2*).

To evaluate $\frac{\partial \alpha_s}{\partial T}$, it is assumed that $\alpha_s = \alpha_s(T,\mu)$, with $\mu = \cos$ (zenith angle), such that

$$\frac{\partial \alpha_s}{\partial T} = \frac{d\alpha_s}{dT} - \frac{\partial \alpha_s}{\partial \mu} \frac{d\mu}{dT} \tag{50}$$

with the second term on the right-hand side constituting a zenith angle correction. For our present purposes, it is sufficient to compute $\frac{d\alpha_s}{dT}$ and $\frac{\partial \alpha_s}{\partial T}$ for each latitude zone in the northern and southern hemisphere, and to apply the zenith angle corrections of the northern hemisphere (which Lian and Cess considered only) also to the southern hemisphere. In their paper, Lian and Cess explain in detail how these values are derived. We also assume $\frac{\partial \alpha_s}{\partial T} = 0$ for latitudes between 40°N and 40°S. The total derivative $\frac{d\alpha_s}{dT}$ is determined from annual zonal data for $\alpha_s(x)$ (Vonder Haar and Ellis 1975) using our surface temperature set as given in *Table 1*. All respective terms are summarized in *Table 2*.

It remains to determine $\frac{\partial \alpha_c}{\partial T}$ and, as with α_s, it is assumed that $\alpha_c = \alpha_c(T,\mu)$. Lian and Cess simply rephrased α_c empirically as $\alpha_c = \alpha_c(\alpha_s,\mu)$ by employing a linear least-squares fit to each hemisphere separately:

$$\alpha_c(\text{NH}) = 0.641 + 0.258\ \alpha_s - 0.494\ \mu \tag{51a}$$

$$\alpha_c(\text{SH}) = 0.691 + 0.219\ \alpha_s - 0.619\ \mu\ . \tag{51b}$$

It should be noted that the above equations uncouple the dependence of α_c upon surface temperature (through α_s) and zenith angle. Furthermore, they indicate the hemispherical percentages of the ice-albedo effect (74% for NH, 78% for SH) which are being screened by clouds for the cloud-covered portions of the hemispheres. From Eq. (49) and Eqs. (51a), (51b), we obtain

$$\frac{\partial \alpha}{\partial T} = \begin{cases} [1 - 0.742\ A_c(x)] \dfrac{\partial \alpha_s}{\partial T} & \text{NH} \quad (52a) \\ \text{for} & \\ [1 - 0.781\ A_c(x)] \dfrac{\partial \alpha_s}{\partial T} & \text{SH} \quad (52b) \end{cases}$$

Table 2. Mean annual zonal data of the refined EBM.

Zone	Latitude	A_c [1]	α_s [2]	$\frac{d\alpha_s}{dT}$ in $\frac{1}{°C}$	$\frac{\partial\alpha_s}{\partial\mu}\cdot\frac{d\mu}{dT}$ [3] in $\frac{1}{°C}$	$\frac{\partial\alpha_s}{\partial T}$ [4] in $\frac{1}{°C}$	$\frac{\partial\alpha}{\partial T}$ [5] in $\frac{1}{°C}$	a [6]	IR [7] in $\frac{W}{m^2}$	z [8] in m	HT [9] in $\frac{W}{m^2}$
1	90–80° N	0.55	0.520	−0.0237	−0.0007	−0.0230	−0.0136	0.3590	176.3	137	−95.3
2	80–70° N	0.61	0.411	−0.0203	−0.0010	−0.0192	−0.0105	0.4145	178.6	220	−79.9
3	70–60° N	0.64	0.304	−0.0128	−0.0018	−0.0110	−0.0058	0.4225	188.0	202	−58.7
4	60–50° N	0.64	0.226	−0.0071	−0.0027	−0.0044	−0.0023	0.4121	200.3	296	−35.1
5	50–40° N	0.57	0.201	−0.0036	−0.0027	−0.0008	−0.0005	0.3613	217.7	382	−13.7
6	40–30° N	0.47	0.176	0.0000	0.0000	0.0000	0.0000	0.3090	239.1	496	10.7
7	30–20° N	0.41	0.170	0.0000	0.0000	0.0000	0.0000	0.2720	255.8	366	28.2
8	20–10° N	0.44	0.142	0.0000	0.0000	0.0000	0.0000	0.2480	258.4	146	33.5
9	10– 0° N	0.51	0.150	0.0000	0.0000	0.0000	0.0000	0.2540	252.7	158	34.6
10	0–10° S	0.50	0.588	0.0000	0.0000	0.0000	0.0000	0.2410	264.2	154	33.6
11	10–20° S	0.47	0.528	0.0000	0.0000	0.0000	0.0000	0.2360	263.9	121	28.5
12	20–30° S	0.47	0.339	0.0000	0.0000	0.0000	0.0000	0.2510	258.5	156	19.6
13	30–40° S	0.54	0.220	0.0000	0.0000	0.0000	0.0000	0.2960	245.2	106	4.0
14	40–50° S	0.65	0.163	−0.0057	−0.0027	−0.0030	−0.0015	0.3726	226.2	5	−17.7
15	50–60° S	0.79	0.140	−0.0098	−0.0027	−0.0071	−0.0027	0.4339	204.3	5	−38.7
16	60–70° S	0.77	0.136	−0.0110	−0.0018	−0.0092	−0.0037	0.4877	189.4	388	−60.5
17	70–80° S	0.56	0.140	−0.0060	−0.0010	−0.0050	−0.0028	0.5191	167.0	1420	−108.0
18	80–90° S	0.47	0.143	−0.0047	−0.0007	−0.0040	−0.0025	0.5103	152.1	2272	−129.8

Table 2 continued:

1) Cloud cover fraction; from Cess (1976).

2) Clear-sky albedo; from Cess (1976).

3) Zenith angle correction; from Lian and Cess (1977).

4) Dependence of clear-sky albedo on surface temperature; from Eq. (50).

5) Dependence of effective albedo on surface temperature; from Eqs. (52a), (52b).

6) From Eq. (53) when tuned against observations.

7) Calculated IR flux; from Eqs. (56a), (56b).

8) Mean height of latitude belt i above sea surface level; from Sellers (1969).

9) Calculated net horizontal energy transport (*cf. Table 1*) with surface temperatures corrected to sea surface level according to Eq. (57) and with $\gamma = 2.99\ \mathrm{W\,m^{-2}\,^{\circ}C^{-1}}$ from a least-squares fit.

Similar to Section 3.1., the zonal albedo is then determined from

$$\alpha(x) = \frac{\partial \alpha}{\partial T}(x)\,T(x) + a(x) \tag{53}$$

where the temperature-independent parameter $a(x)$ is tuned to fit the observed zonal planetary albedos. Note that the dependency of the effective albedos on T and μ is substituted by a dependency on x. As can be seen from *Table 2*, except for the two most northern latitude belts, the absolute values of $\frac{\partial \alpha}{\partial T}$ are significantly lower than Sellers' value of $0.009^{\circ}C^{-1}$ in his albedo parameterization. This feature leads to an increased global stability (Warren and Schneider 1979, and *cf.* also Section 4.1.).

Following Lian and Cess, we also do not assume the cloud cover to depend on temperature. Observationally, $\frac{dA_c}{dT}$ is positive for the seasonal cycle in some latitude zones and negative in others. Thus it is not clear at all how cloud cover would change with a change in temperature (Warren and Schneider 1979).

Finally, for use in our refined EBM, Eq. (53) is rewritten in a time-dependent fashion with respect to a change in surface temperature

$$\Delta\alpha(x,t) = \frac{\partial \alpha}{\partial T}(x)\,\Delta T(x,t) \tag{54}$$

where $\frac{\partial \alpha}{\partial T}$ is taken to be constant in time.

(b) Infrared flux

Cess (1976) assumed the outgoing IR flux at the top of the atmosphere also to be a linear function of surface temperature. He re-evaluated the linear parameterization using more recent IR data from satellites and cloudiness data. By employing annual and zonal average data for the northern and southern hemisphere separately, he found

$$\mathrm{IR}(x) = \begin{cases} 257 + 1.63\ T(x) - [91 + 0.11\ T(x)]\,A_c(x) & \text{NH} \quad (55a) \\ \text{for} \\ 262 + 1.64\ T(x) - [81 + 0.09\ T(x)]\,A_c(x) & \text{SH} \quad (55b) \end{cases}$$

(in $\mathrm{W\,m^{-2}}$) from a least-squares fit where A_c is the fractional cloud cover mentioned above. Following Warren and Schneider (1979), the fourth term on the right-hand side can be neglected because its contribution to the entire right side does not exceed 1.5%. Thus employing $\mathrm{IR}(x) = A + BT(x) + kA_c(x)$ to each hemisphere where k is an empirical constant, we obtain for today's climate

$$\mathrm{IR}(x) = \begin{cases} 254.2 + 1.68\ T(x) - 90\ A_c(x) & \text{NH} \quad (56a) \\ \text{for} \\ 257.1 + 1.67\ T(x) - 73\ A_c(x) & \text{SH} \quad (56b) \end{cases}$$

(*cf. Table 2* and *Figure 5*). As in Section 3.1., we also assume Eqs. (56a), (56b) to be applicable in the form $\Delta IR(x,t) = \Delta A(t) + B\Delta T(x,t)$ when used for a climatic change simulation.

(c) Horizontal energy transport

Budyko's (1969) formula of the net horizontal energy transport has basically been retained. We have only introduced Sellers' (1969) height corrections ($z(x)$; *cf. Table 2*) and lapse rate ($0.0065\,^{\circ}C\,m^{-1}$) to relate our surface temperatures (ST) to sea surface level (SST) according to

$$T_{SST}(x,t) = T_{ST}(x,t) + 0.0065\,\frac{^{\circ}C}{m} \cdot z(x) \tag{57}$$

for which we found $\gamma = 2.99\ W\,m^{-2}\,^{\circ}C^{-1}$ from a least-squares fit and $15.86\,^{\circ}C$ for today's global average temperature on sea surface level (*cf. Figure 6*). Being aware of the fact that Budyko's parameterization of the net horizontal energy transport will be the first one to be changed completely as soon as our EBM approaches a finer subdivision (atmosphere, land, ocean), we found Budyko's refined parameterization satisfactory enough with respect to our present level of modeling. A least-squares fit of a thermal–diffusive transport with a constant diffusion coefficient (Eq. (33)) proved even worse for both temperature levels.

4. RESULTS

In this chapter we present the results of simulations from four different energy balance models under various radiative forcing conditions. The energy balance models are the two-hemispherical EBM of IMAGE (Section 3.2.), the two-hemispherical and the 18-latitudinal version of the basic EBM (Section 3.3.2.), and the 18-latitudinal version of the refined EBM (Section 3.4.). The EBM in the climate module of IMAGE is coupled to an advective–diffusive deep ocean and calculates the hemispherical changes in surface temperature. This coupling with the deep ocean is the main difference between the EBM of IMAGE and the other energy balance models mentioned. It has a far-reaching consequence in that the radiative forcing is partly being taken up by the deep ocean which by its long turnover time damps the response of the climate system to radiative forcing whereas the energy balance models set up in this paper respond on a much shorter time scale.

Both *transient* and *time-dependent simulations* have been performed with all four energy balance models. As already explained (Section 3.3.), the first refers to a simulation with an instantaneous doubling of atmospheric CO_2 concentration at the beginning; the model is then run for some time period to approach its equilibrium. The second, the time-dependent simulation experiment, represents a model run under gradually increasing greenhouse gas concentrations, implying an increasing radiative forcing scenario (scenario A of the IPCC (1990)). In order to compare all four energy balance models we use the globally averaged change in surface temperature as a reference.

4.1. Transient Simulations

In these experiments the temperature effect of a sudden *switch-on* instantaneous CO_2 doubling ($\Delta Q_{2\times CO_2} = 4.32\ W\,m^{-2}$) is examined. An important reason for examining switch-on cases is the need to better understand the response of the climate system to external forcing. *Figure 7* shows the hemispherical temperature responses of IMAGE and the globally averaged temperature response of the two-hemispherical basic EBM (Eq. (46)). The hemispherical responses of the latter have not been shown because they do not resolve visibly from one another on the compressed time axis used. The temperature responses of both models approach equilibrium temperatures termed *climate sensitivities* which are characterized by $\Delta T(2\times CO_2)$. According to the IPCC, this quantity falls within a range of 1.5 to 4.5°C, with a best estimate of 2.5°C. By setting the global feedback parameter in IMAGE, λ_0(IMAGE), to $1.728\ W\,m^{-2}\,°C^{-1}$, IMAGE reproduces $\Delta T(2\times CO_2) = 2.5°C$ exactly (Section 3.3.1.). The corresponding value of the two-hemispherical EBM is 2.43°C. This value is ultimately determined by the IR parameter $B = 1.78\ W\,m^{-2}\,°C^{-1}$ (*cf.* Eqs. (34a), (34b)).

The two-hemispherical EBM reaches the equilibrium temperature relatively quickly, the reason for which is the missing deep ocean. Its globally averaged response encompasses two temperature relaxation processes which result from the hemispherical breakdown of the system. They refer to relaxation processes on a global and on a hemispherical scale. Note that there is a little difference between the e–folding times of the globally averaged ($\bar{\tau}_0 = 3.83\,y$) and the global temperature response ($\tau_0 = 3.84\,y$; Eq. (27)). This is in agreement with other authors. (For instance, when comparing an annually averaged seasonal EBM with an annual EBM, North *et al.* (1981) also found the first one to comprise more information than the second one.) The hemispherical e–folding times of IMAGE are 20y (NH) and 23y (SH), respectively. Even after 200 years the climate system is still not in its equilibrium due to the deep ocean.

The transient simulations of the 18-latitudinal version of both the basic and the refined EBM are depicted in *Figures 8* and *9*. If we were to generalize our findings in Section 3.3.2., we would find that the temperature responses of both models, whether latitudinal or globally averaged, are superpositions of up to 18 different relaxation processes induced by the latitudinal breakdown of the system. An important feature of both models is the relative high temperature sensitivity, 4.41°C for the globally averaged basic EBM and 3.11°C for the globally averaged refined EBM. The reason for the increased climate sensitivity of the 18-latitudinal basic EBM compared to its two-hemispherical version is that the albedo-temperature feedback is now coming into the latitudinal feedback parameter λ_i (*cf.* Eq. (31)). In the two-hemispherical basic EBM no change in albedo was assumed because of the hemispherical temperatures being greater than 10°C. The parameter $\left[\frac{\partial \alpha}{\partial T}\right]_i$ which is uniformly $-0.009°C^{-1}$ for Sellers' (1969) parameterization and latitude-dependent in mid to high latitudes for Lian and Cess' (1977) parameterization, is of great importance for the climate sensitivity as can readily be seen from the matrix equations (32a), (32b). A smaller feedback parameter implies a greater climate sensitivity latitudinally (and thus a smaller global stability) and vice versa. As to be expected, the latitudinal climate sensitivities of the 18-latitudinal refined EBM are generally lower than the corresponding climate sensitivities of the basic EBM, except for the North Pole. Here

Lian and Cess' calculations yield even a smaller albedo-temperature feedback ($-0.0136°C^{-1}$) than Sellers'. The different global stabilities can also be inferred from the respective *e*–folding times of the globally averaged temperature responses. They are 5y for the refined EBM and 7y for the basic EBM. However, due to the missing deep ocean both models still act on a time scale much shorter than that of IMAGE.

4.2. Time-Dependent Simulations

Based on the *Business–as–Usual scenario* (scenario A of the IPCC (1990)[1]), IMAGE simulates in a time-dependent fashion the atmospheric greenhouse gas concentration and the induced radiative forcing (*cf. Figure 10*). With the best judged parameters by the IPCC, IMAGE calculates increases in hemispherical surface temperature of 4.1°C (NH) and 4.0°C (SH), respectively, in 2100. The final temperature increase of the globally averaged two-hemispherical basic EBM is 4.9°C[2]. For reasons of completeness, the response of the globally averaged equilibrium temperature is also shown. This temperature increase is calculated by IMAGE where it is assumed that the climate system is constantly in equilibrium (no storage of heat). It gives an indication of how marginal the effect of the heat capacity (mixed layer, only) in the two-hemispherical basic EBM is compared to that of the deep ocean in IMAGE. In 1985, e.g., IMAGE simulates a temperature response of about 0.65°C which corresponds to the measured global mean temperature rise of 0.5 to 0.7°C (Schlesinger 1986, Wigley 1987, Hansen *et al.* 1988) while the two-hemispherical basic EBM gives already an increase of about 1.0°C. This emphasizes that the incorporation of a deep ocean is needed for more realistic simulations based on different emission policies.

In *Figures 11* and *12* the temperature responses of both the 18-latitudinal basic and refined EBM are depicted. Their globally averaged responses reveal higher temperature increases than IMAGE. In 1985 and 2100 the increases are 1.75 and 7.22°C for the basic EBM and 1.25 and 5.9°C, respectively, for the refined EBM. This is due to the higher climate sensitivities defined above. They are strongly influenced by the parameterization of the albedo-temperature feedback as can be seen in *Figures 13* and *14* which show latitudinal temperature changes for three years: 1990, 2050 and 2100. It is basically the latitudinal variation of $Q_0 S_i \left[\frac{\partial \alpha}{\partial T}\right]_i$ which we see here and which ultimately determines the latitudinally varying temperature responses in *Figures 11* and *12*.

[1] In the Business–as–Usual scenario (scenario A) the energy supply is coal-intensive and on the demand side only modest efficiency increases are achieved. Carbon monoxide controls are modest, deforestation continues until the tropical forests are depleted, and agricultural emissions of methane and nitrous oxide are uncontrolled. For CFCs the Montreal Protocol is implemented albeit with only partial participation.

[2] We have used today's hemispherical or latitudinal surface temperatures, respectively, as the 1900–starting temperatures for the two-hemispherical basic EBM, and for both the 18-latitudinal basic and refined EBM. Since we calculate temperature differences, this is only of importance when a temperature condition is checked, e.g., the albedo-temperature condition in Eqs. (11) and (36) which, in turn, only affects the 18-latitudinal basic EBM. If the starting temperatures would have been somewhat lower, some latitudes would be influenced a little later by the respective condition. At the present level of modeling, we do not consider this a serious shortcoming.

5. CONCLUSIONS AND OUTLOOK

It was the objective of this paper to lay the scientific and numerical basis for a two-dimensional energy balance model which resolves latitude and height, and the output of which is surface temperature and precipitation in 10° latitude belts. So far, we have examined the first level of modeling: a one-dimensional EBM which resolves mean annual latitudinal temperatures and which belongs to the Budyko–Sellers type of energy balance models.

The temperature projections derived with this relatively simple EBM are still not realistic mainly due to the severe shortcoming that no deep ocean for heat uptake has been taken into consideration. However, because of its simplicity we were able to study the linkage to IMAGE and to explore the relative importance of various parameterizations of the albedo, the IR flux and the net horizontal energy transport. We also gained analytical insights on the global and latitudinal scales into important model parameters such as the equilibrium sensitivity parameter, the feedback parameter and the climate sensitivity, and how they determine the behavior of the model.

The present steering mechanism which is based on the radiative forcing needs to be changed in future so that the atmospheric greenhouse gas concentrations calculated by IMAGE can be directly used. This is foreseen for the next level of modeling and would help to prevent accounting twice for some effects; first, by the radiative forcing and, second, by the parameterizations used in the EBM. The new steering, however, requires an atmospheric radiative transfer model and, in the long run, also an estimate on the spatial distribution of the greenhouse gases in the atmosphere.

Both the 18-latitudinal basic and refined EBM produce rather high climate sensitivities. This is due to the albedo-temperature feedback which, in turn, strongly influences the latitudinal feedback parameter and thus the global stability. It is $Q_0 S_i \left[\frac{\partial \alpha}{\partial T}\right]_i$, the product of the solar constant with the meridional distribution of solar radiation and the albedo-temperature feedback parameter, which basically determines the latitudinal variation of the temperature responses in both transient and forced simulations. This indicates that in the next phase of modeling much attention has to be paid to a good parameterization of albedo with respect to different surface types; this can then be linked to the radiative transfer scheme mentioned above.

Summarizing, the EBM set up in this paper needs to be further developed in order to achieve more realistic mean annual temperature projections. The EBM to be modeled next should be coupled to a deep ocean model and consist of a multilayer atmosphere over land and ocean.[3] Sea ice and snow also need to be included in this EBM. A radiative transfer scheme should allow for a direct mode of steering through the atmospheric greenhouse gas concentrations as being compiled by IMAGE. The EBM of the next modeling phase will also be described in a future RIVM/IIASA joint publication.

[3]For the deep ocean the two-dimensional advective–diffusive ocean model of den Elzen and de Haan (1991) should serve as a basis.

FIGURES

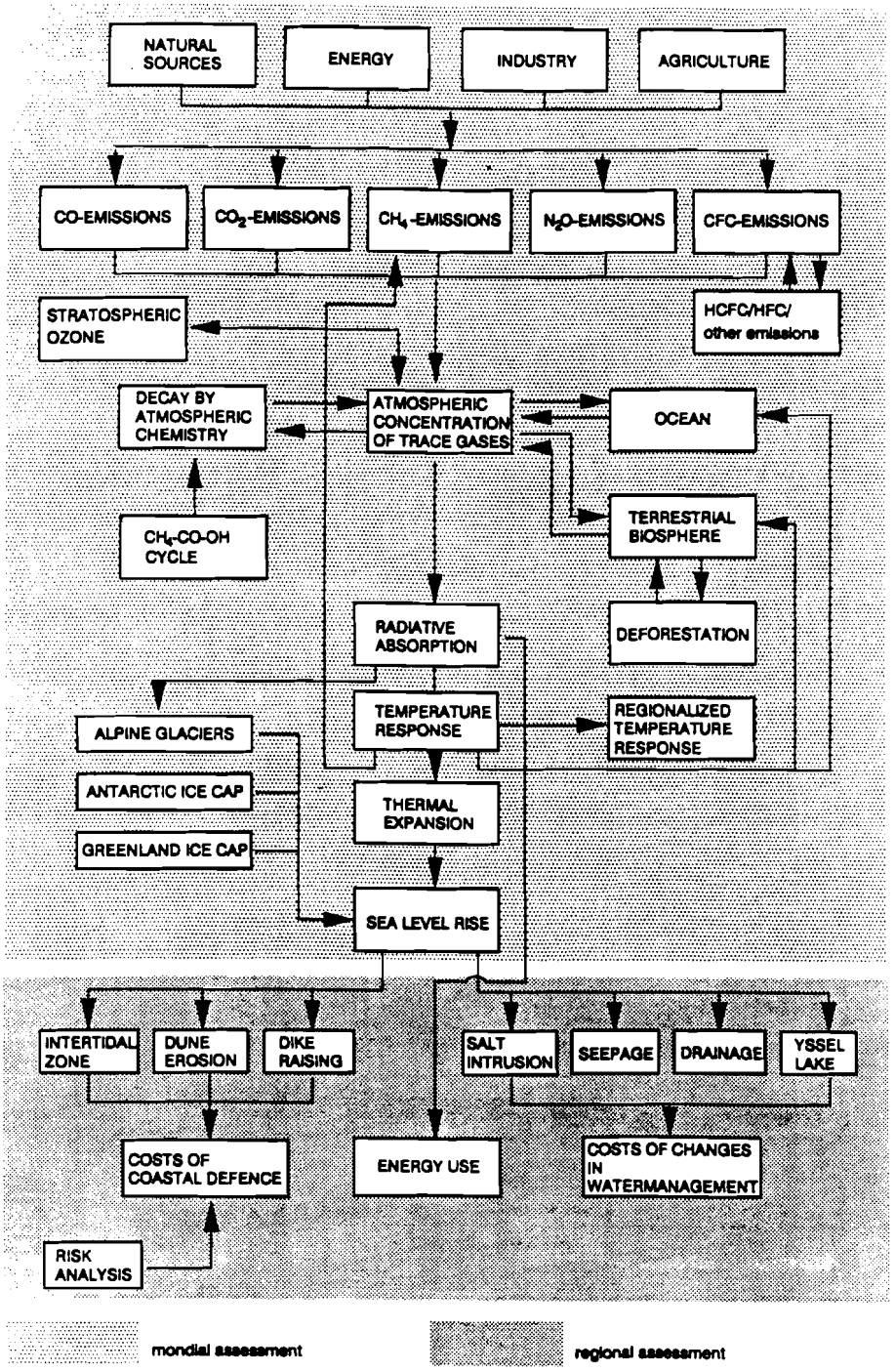

Integrated Model for the Assessment of the Greenhouse Effect (IMAGE)

Figure 1. Integrated Model to Assess the Greenhouse Effect (IMAGE; Rotmans 1990).

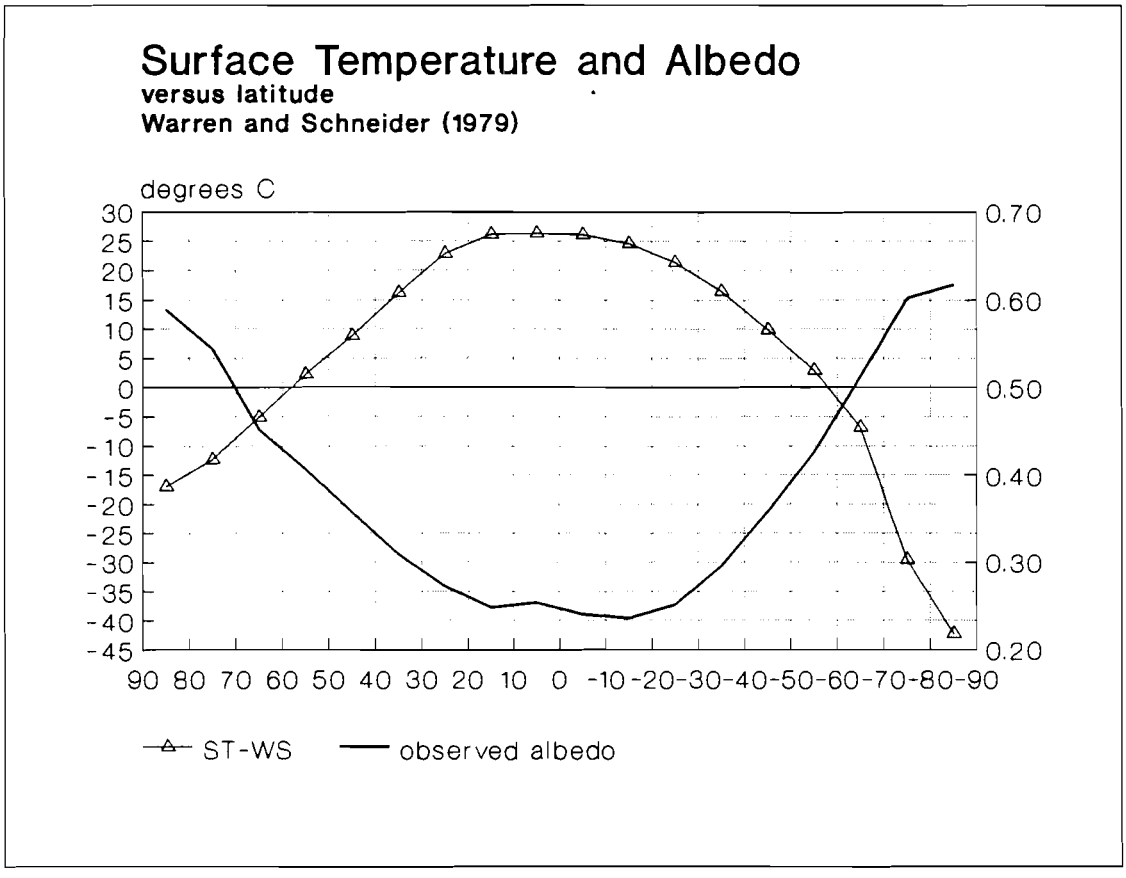

Figure 2. Observed and smoothed mean annual surface temperature (from Warren and Schneider 1979) and observed mean annual planetary albedo (from Ellis and Vonder Haar 1976) vs. latitude.

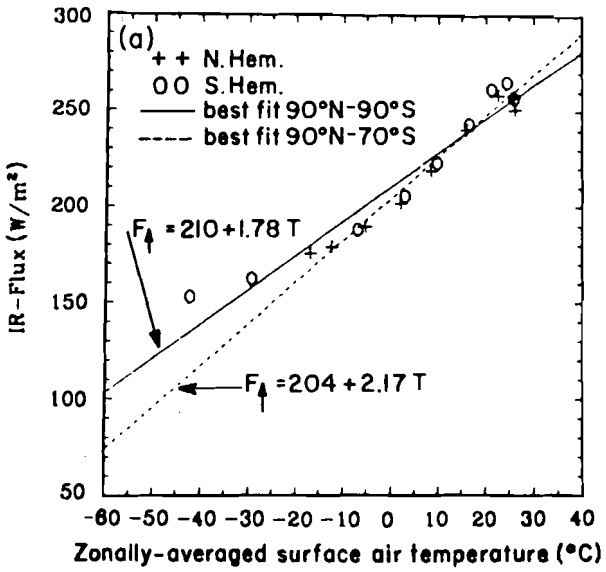

Figure 3. Mean annual values of observed outgoing IR flux as a function of surface temperature vs. latitude. IR flux data are from Ellis and Vonder Haar (1976). Plus marks indicate northern hemisphere; circles, southern hemisphere. Solid line: best fit to all points with an area-weighted mean deviation from observations of 7.13 $W m^{-2}$. Dashed line: best fit to all points excluding 70–90°S. This figure is taken from Warren and Schneider (1979) (their Figure 5(a)).

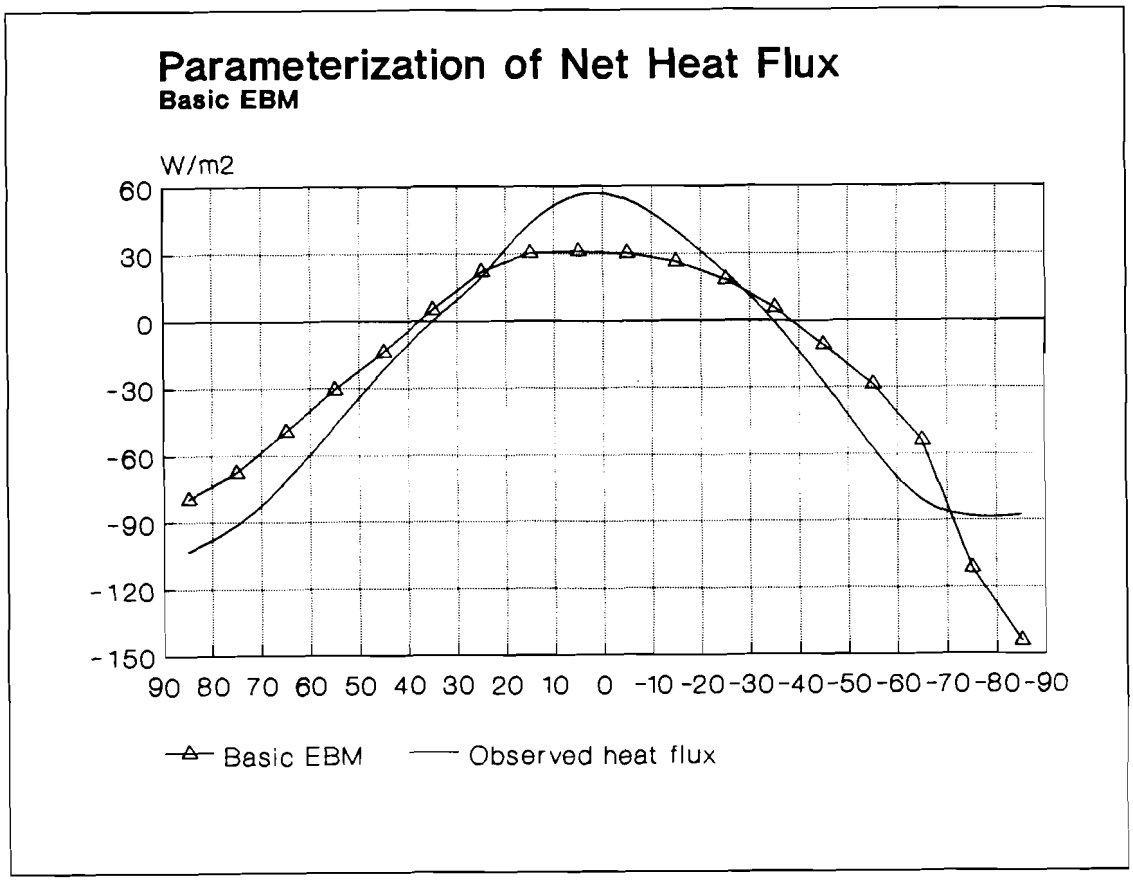

Figure 4. Mean annual net horizontal energy transport vs. latitude. Solid line: observed values of net radiation from Ellis and Vonder Haar (1976). Triangles: net energy transport predicted by Budyko's (1969) linear formula with $\gamma = 2.55\ \mathrm{W\,m^{-2}\,^{\circ}C^{-1}}$ and an area-weighted mean deviation from observations of $15.88\ \mathrm{W\,m^{-2}}$.

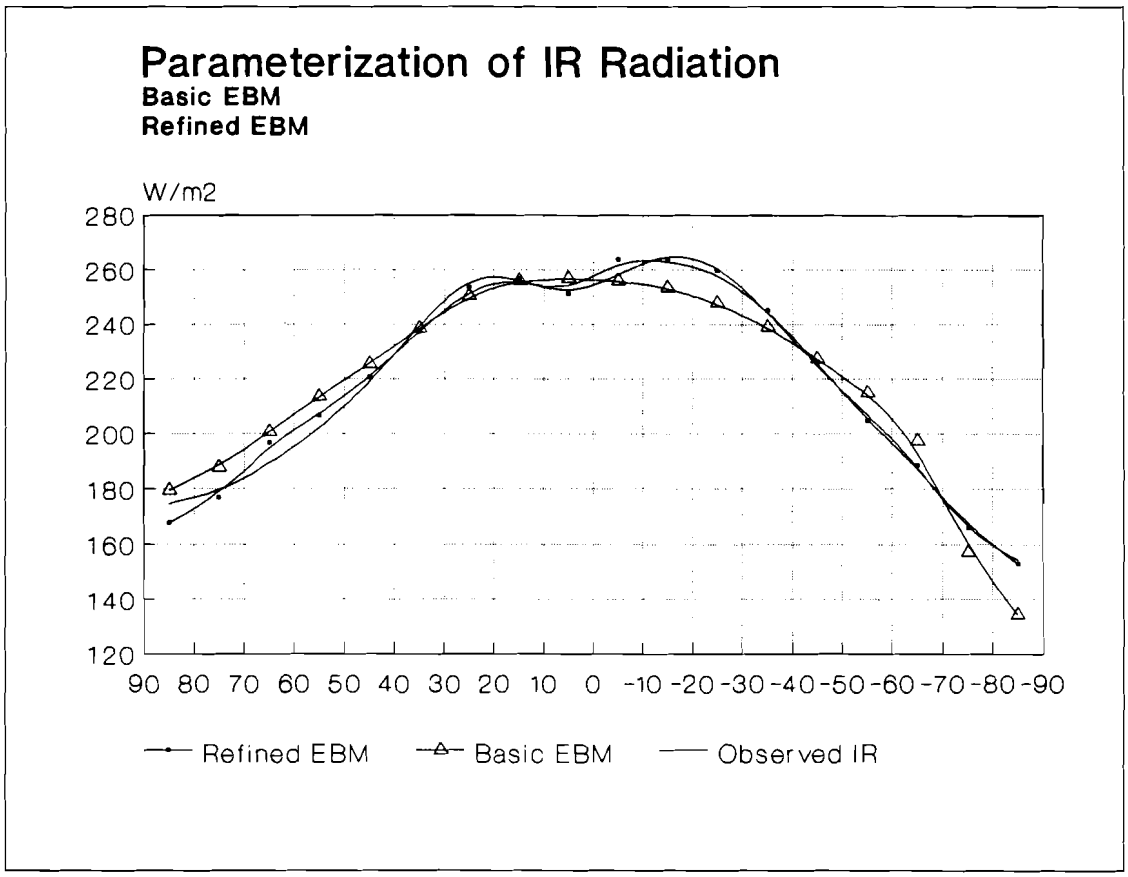

Figure 5. Mean annual IR flux vs. latitude. Observed values and values of the basic IR parameterization are as in *Figure 3*. The area-weighted mean deviation of the refined IR parameterization (Eqs. (56a), (56b)) from observations is 2.24 W m^{-2}.

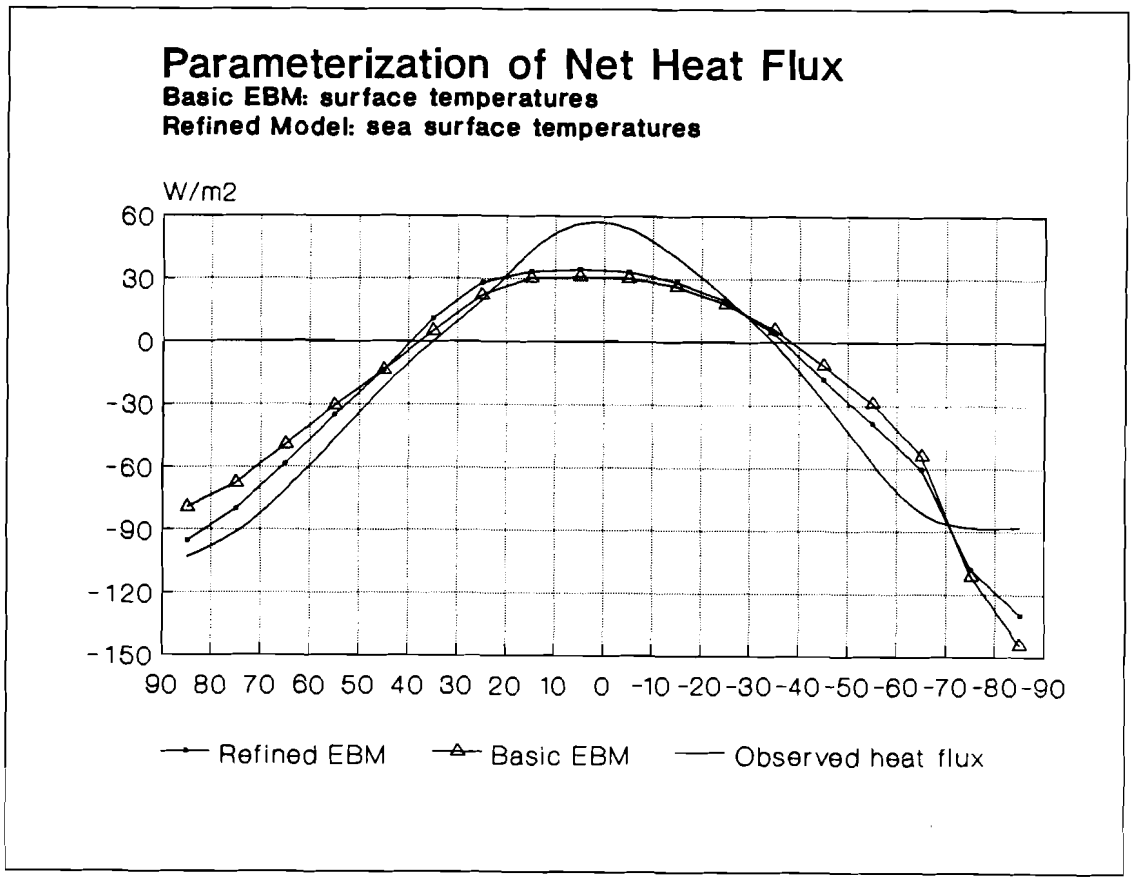

Figure 6. Mean annual net horizontal energy transport vs. latitude. Observed values of net radiation and values of the basic net transport parameterization are as in *Figure 4*. The area-weighted mean deviation of the refined net transport parameterization (with $\gamma = 2.99\ \mathrm{W\,m^{-2}\,^{\circ}C^{-1}}$) from observations is $13.17\ \mathrm{W\,m^{-2}}$.

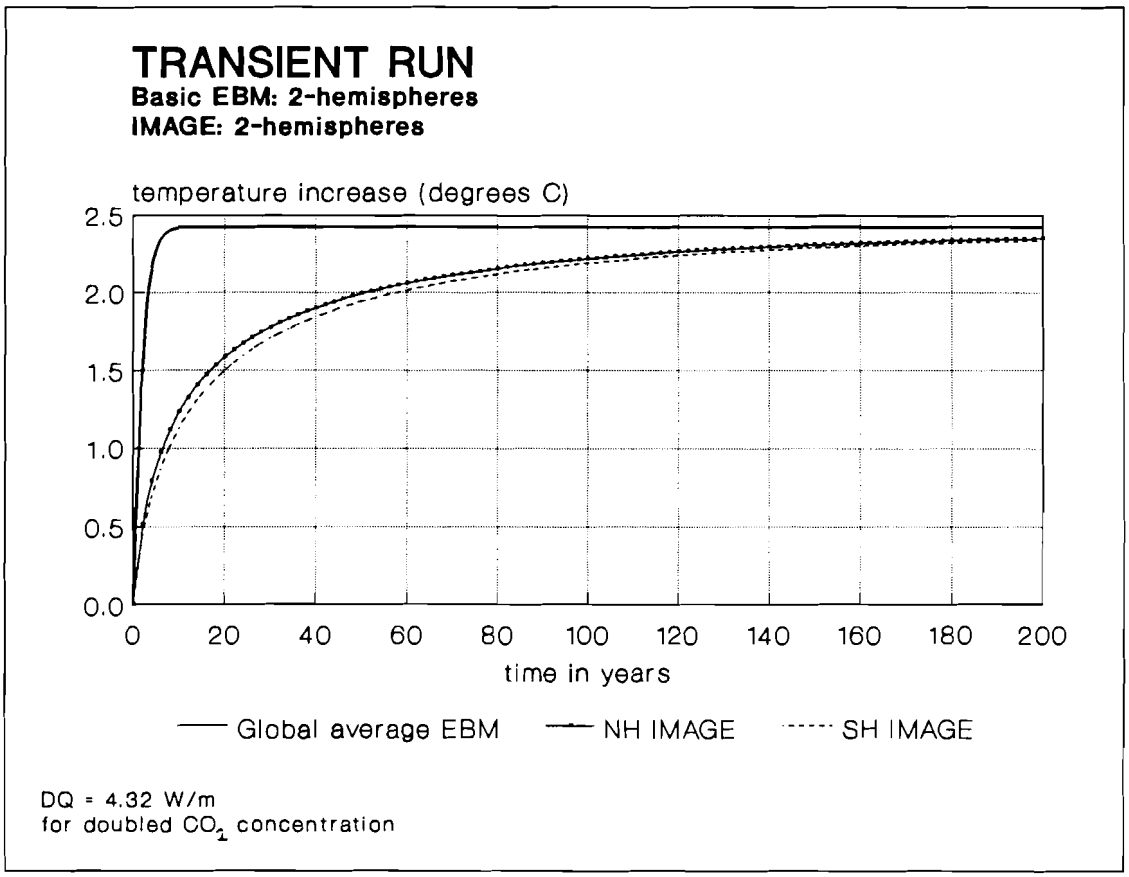

Figure 7. Transient simulations of the northern and southern hemisphere with IMAGE and with the globally averaged two-hemispherical basic EBM (Eq. (46)).

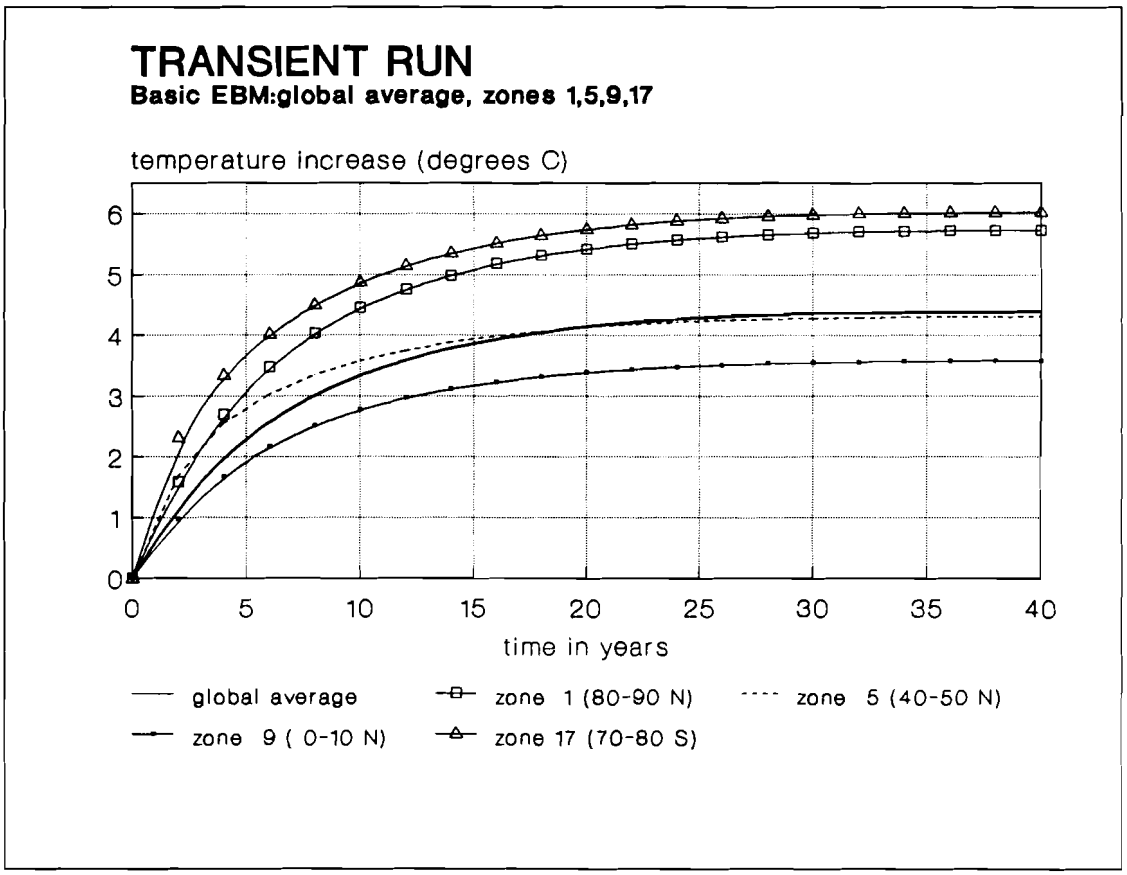

Figure 8. Transient simulation with the 18-latitudinal basic EBM. Depicted are the temperature responses of four different zones and the globally averaged response of all zones.

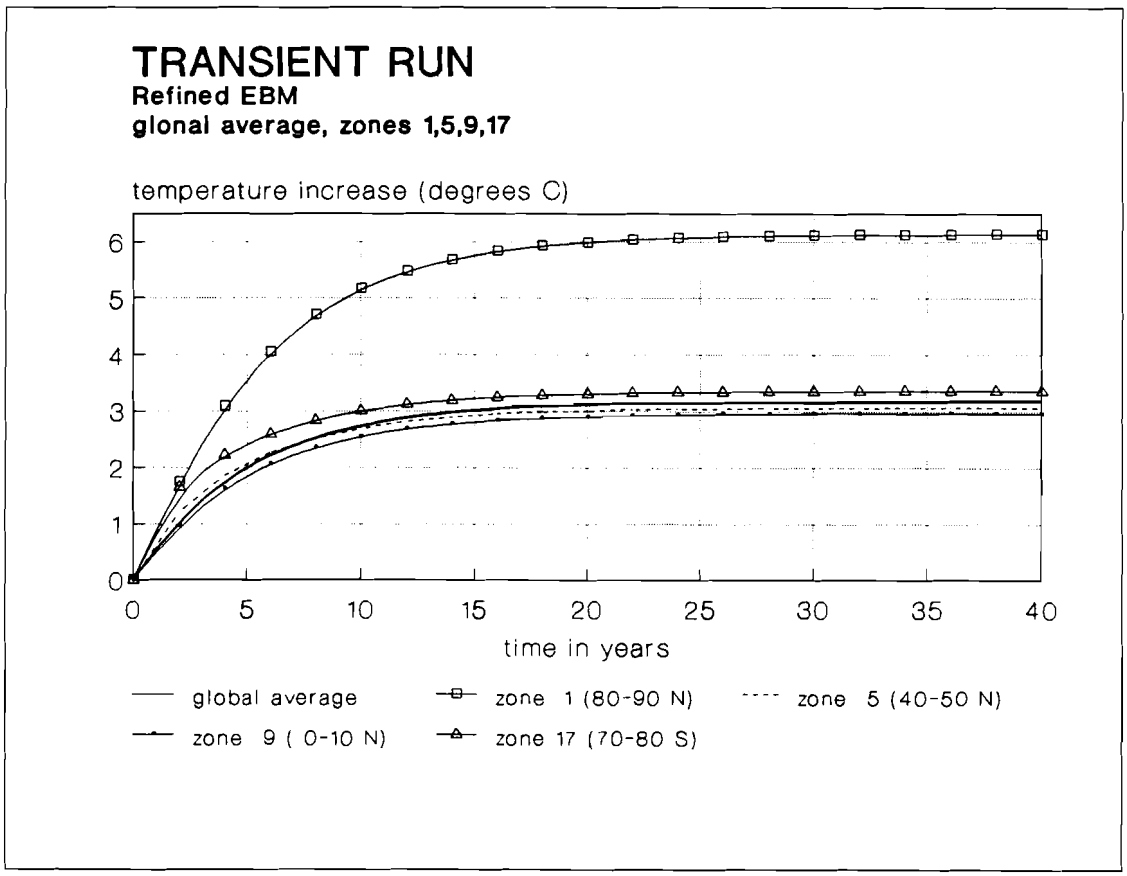

Figure 9. Transient simulation with the 18-latitudinal refined EBM. Depicted are the temperature responses of the same zones as in *Figure 8* and the globally averaged response of all zones.

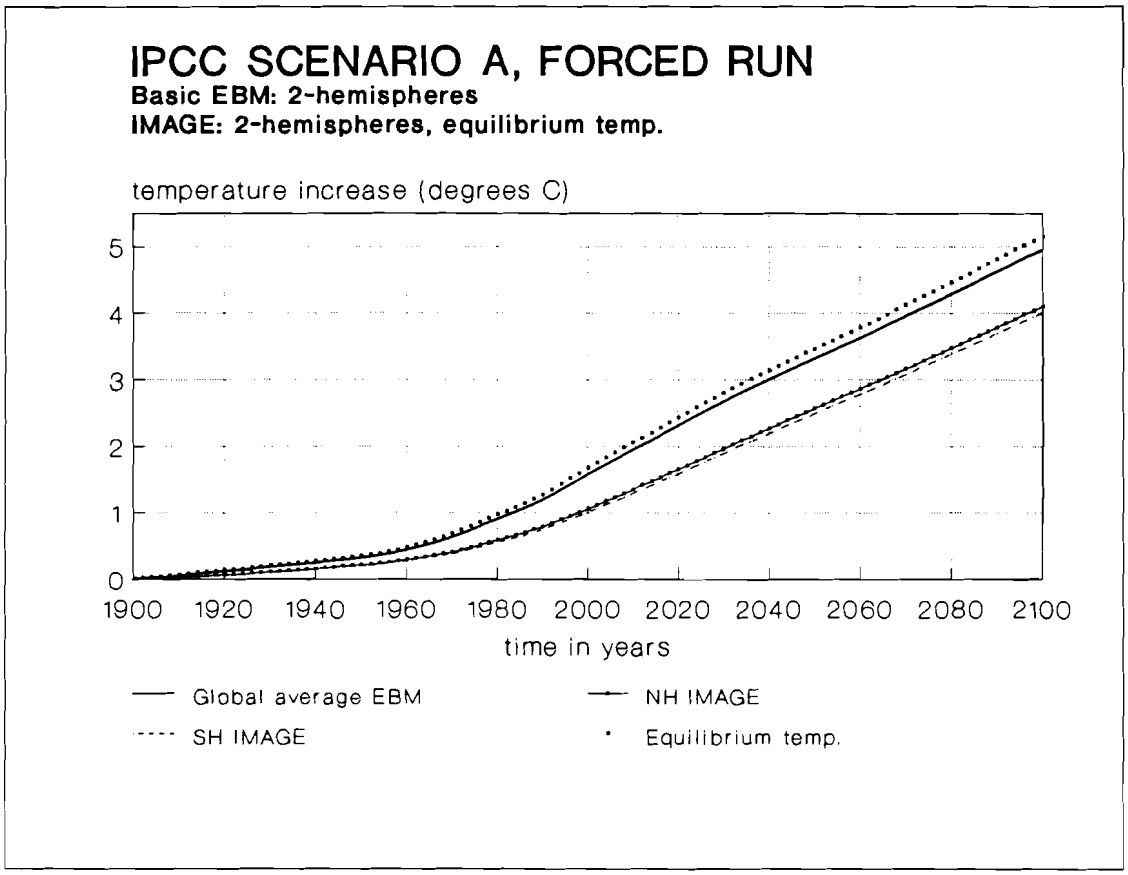

Figure 10. Forced simulations (IPCC scenario A) of the northern and southern hemisphere with IMAGE and with the globally averaged two-hemispherical basic EBM. In addition, IMAGE is also run in a global equilibrium fashion (no storage of heat).

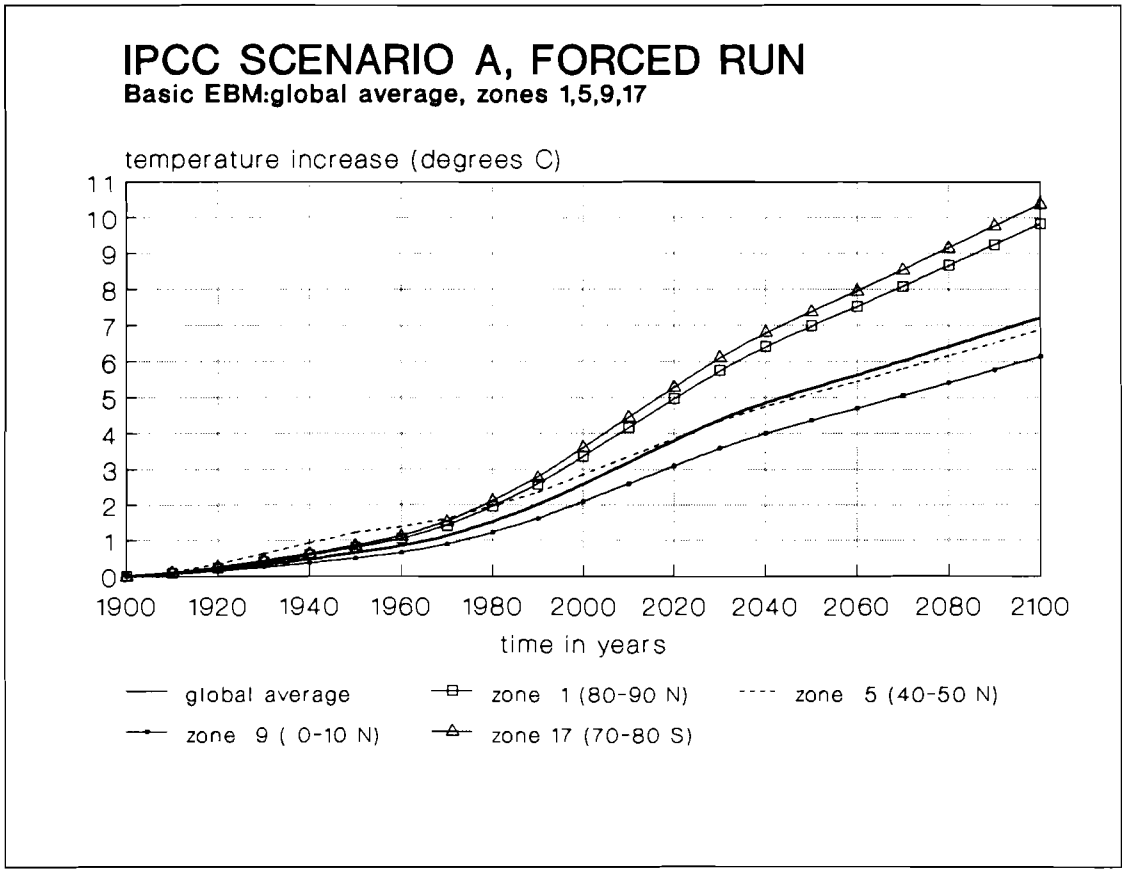

Figure 11. Forced simulation (IPCC scenario A) with the 18-latitudinal basic EBM. Depicted are the temperature responses of four different zones and the globally averaged response of all zones.

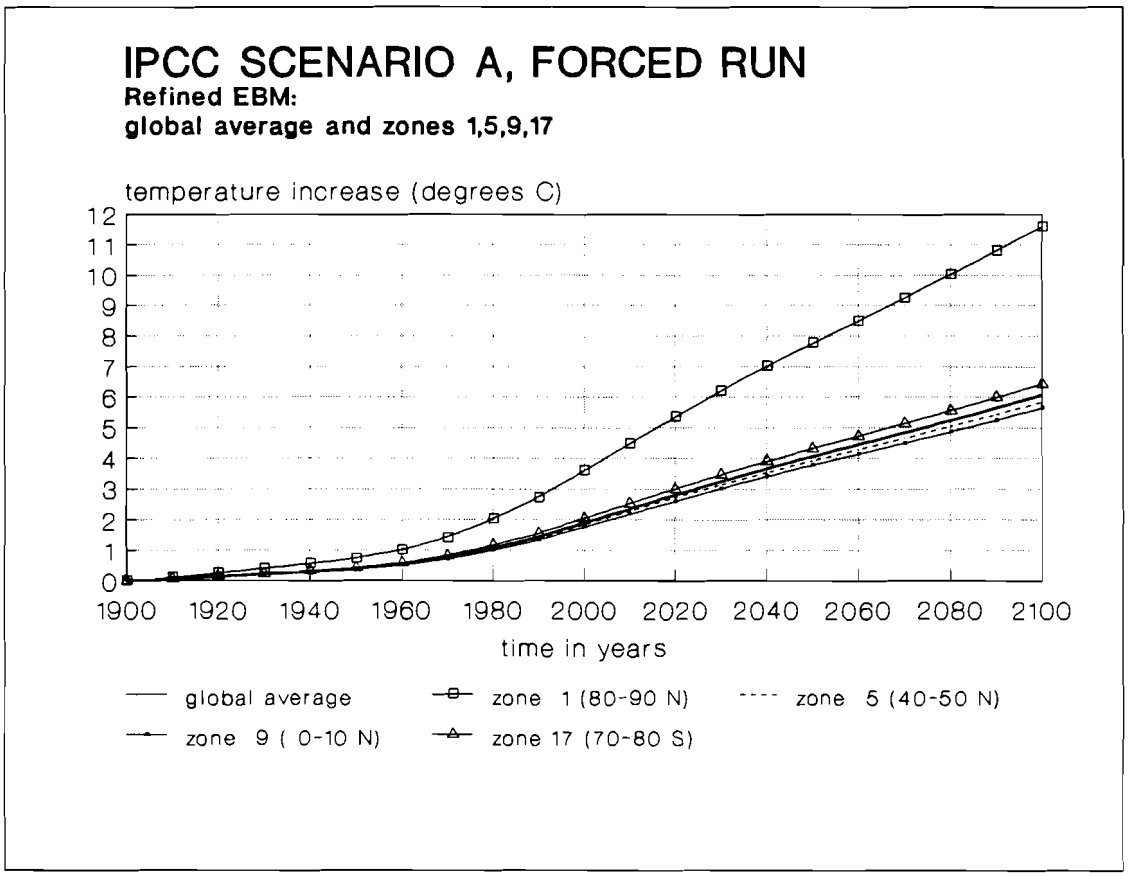

Figure 12. Forced simulation (IPCC scenario A) with the 18-latitudinal refined EBM. Depicted are the temperature responses of the same zones as in *Figure 11* and the globally averaged responses of all zones.

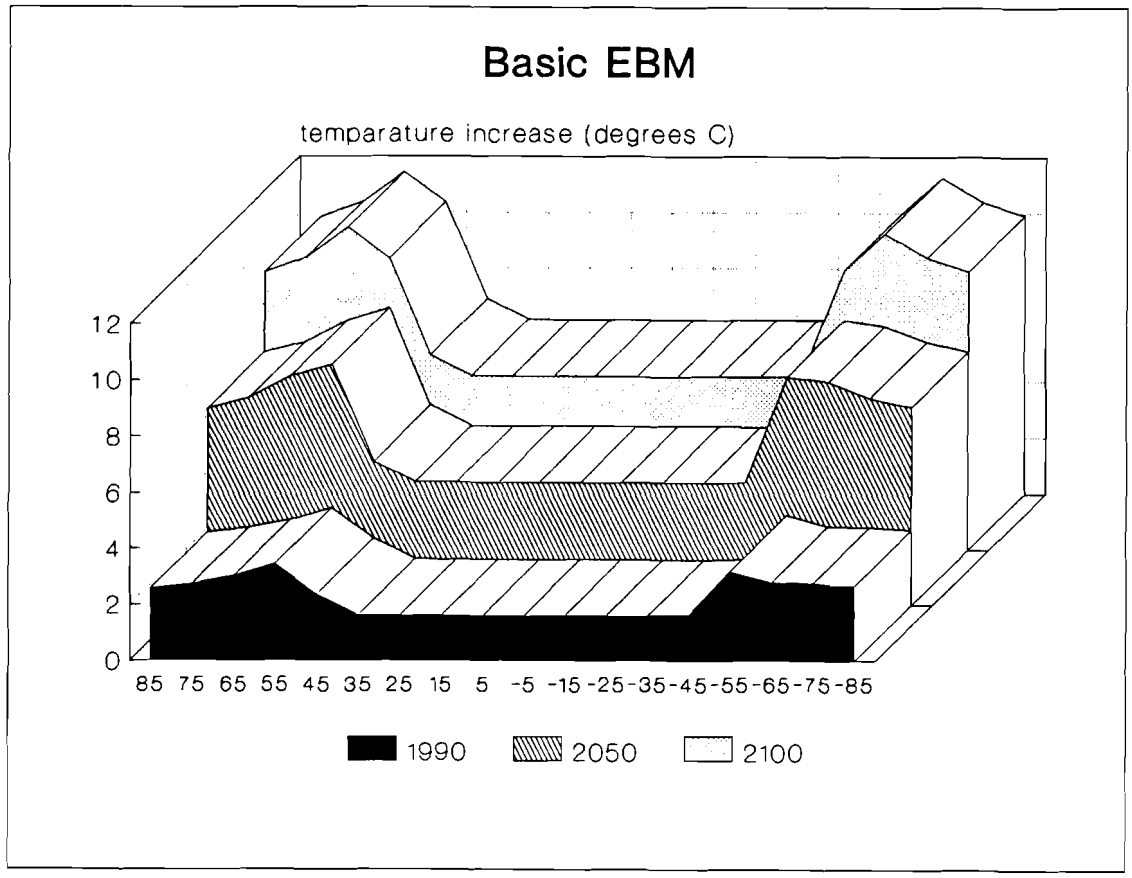

Figure 13. Forced simulation (IPCC scenario A) with the 18-latitudinal basic EBM. Depicted are the latitudinal temperature responses for three time cuts (1990, 2050, 2100) of *Figure 11*.

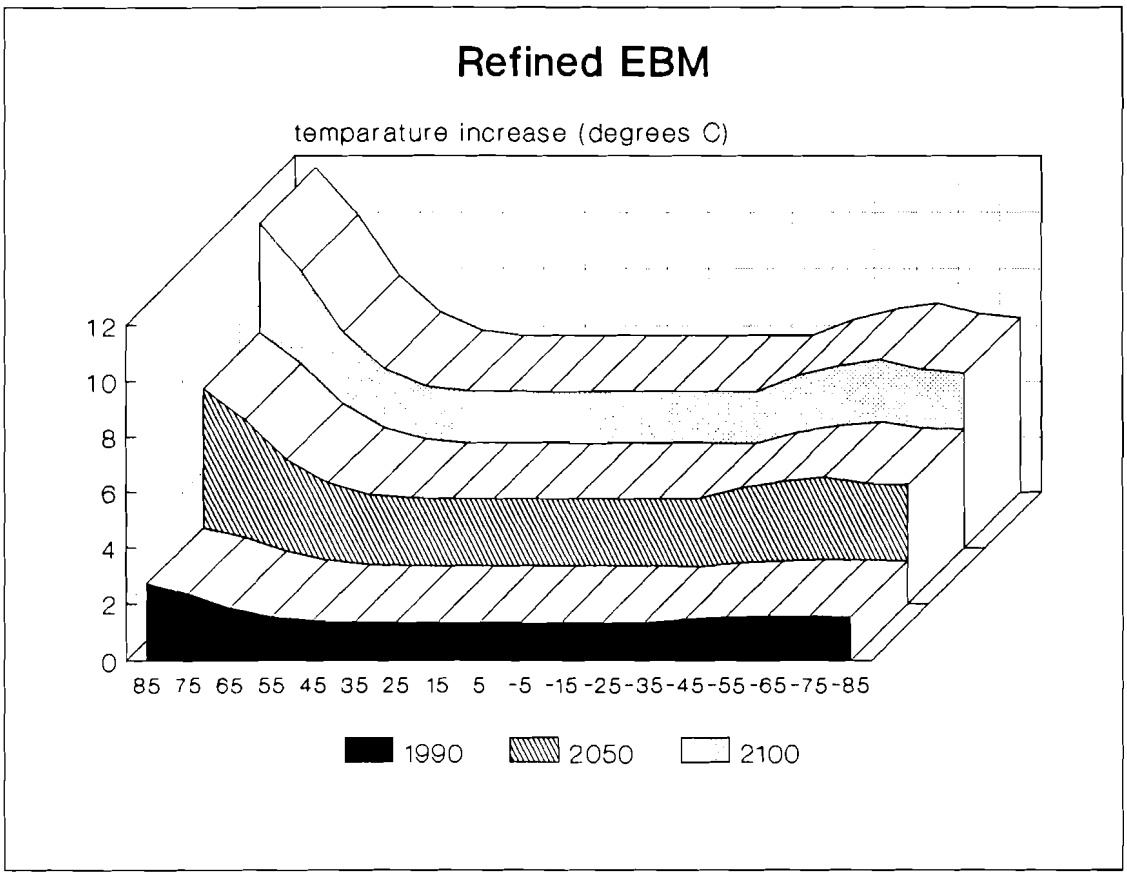

Figure 14. Forced simulation (IPCC scenario A) with the 18-latitudinal refined EBM. Depicted are the latitudinal temperature responses for three time cuts (1990, 2050, 2100) of *Figure 12*.

APPENDIX

(A)

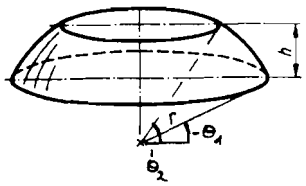

F_o = area of sphere, F_i = area of latitude belt

$$F_i = 2\pi rh = 2\pi r^2(\sin\theta_2 - \sin\theta_1)$$

$$F_o = 4\pi r^2$$

$$f_i = \frac{F_i}{F_o} = \frac{\sin\theta_2 - \sin\theta_1}{2}$$

$$\Rightarrow \sum_{i=1}^{n} f_i = 1 \ .$$

(B) Area-weighting Eq. (9) and adding up yields

$$\sum_{i=1}^{n} f_i\left[R_i \frac{d}{dt} T_i(t)\right] =$$

$$= Q_0 \sum_i f_i S_i - Q_0 \sum_i f_i S_i \alpha_i(t) - \left[A(t) \sum_i f_i + B \sum_i f_i T_i(t)\right] - \gamma\left[\sum_i f_i T_i(t) - T_0(t) \sum_i f_i\right]$$

$$= Q_0(1 - \alpha_0(t)) - (A(t)) + BT_0(t)) \ .$$

Arguing that a global energy balance results exactly in the right side of this equation because the net horizontal energy transport for the earth as a whole is zero, we find

$$R_0 \frac{dT_0(t)}{dt} = \sum_{i=1}^{n} f_i\left[R_i \frac{dT_i(t)}{dt}\right] \ .$$

Equations (16) and (13) can be derived in the same way.

(C) Diagonalizing the matrix equations (32a), (32b) yields

ΔT_1	ΔT_2	
$1 - \frac{\gamma f_1}{\lambda_1}$	$-\frac{\gamma f_2}{\lambda_1}$	$\frac{-\Delta A}{\lambda_1}$
0	$\left[1 - \frac{\gamma f_2}{\lambda_2}\right]\left[1 - \frac{\gamma f_1}{\lambda_1}\right]$	$\frac{-\Delta A}{\lambda_2}\left[1 - \frac{\gamma f_1}{\lambda_1}\right]$
	$-\left[-\frac{\gamma f_2}{\lambda_1}\right]\left[-\frac{\gamma f_1}{\lambda_2}\right]$	$-\frac{-\Delta A}{\lambda_1}\left[-\frac{\gamma f_1}{\lambda_2}\right]$.

Making use of $\lambda_1 = \lambda_2$ and $f_1 = f_2 = \frac{1}{2}$, we find for $\Delta T_2(2 \times CO_2)$

$$\left\{\left[1 - \frac{\gamma f_1}{\lambda_1}\right]^2 - \left[\frac{\gamma f_1}{\lambda_1}\right]^2\right\} \Delta T_2 = \frac{-\Delta A}{\lambda_1}$$

$$\Rightarrow \Delta T_2 = \frac{\frac{-\Delta A}{\lambda_1}}{1 - 2\frac{\gamma f_1}{\lambda_1}} = \frac{-\Delta A}{\lambda_1 - \gamma} = \frac{-\Delta A}{B} \quad ,$$

and for $\Delta T_1(2 \times CO_2)$

$$\left[1 - \frac{\gamma f_1}{\lambda_1}\right] \Delta T_1 + \left[-\frac{\gamma f_1}{\lambda_1}\right] \Delta T_2 = \frac{-\Delta A}{\lambda_1}$$

$$\Rightarrow \Delta T_1 = \left[1 - \frac{\gamma f_1}{\lambda_1}\right]^{-1} \frac{-\Delta A}{\lambda_1} \left[1 - \frac{\frac{-\gamma f_1}{\lambda_1}}{1 - 2\frac{\gamma f_1}{\lambda_1}}\right]$$

$$= \frac{-\Delta A}{\lambda_1 - \gamma} = \frac{-\Delta A}{B} \quad .$$

(D) In order to find the eigenvalues of M_2, we have to determine where the characteristic polynomial of M_2, $\det(M_2 - \alpha I)$ (I = unit matrix), becomes zero:

$$\det(M_2 - \alpha I) = \begin{vmatrix} a_{11} - \alpha & a_{12} \\ a_{21} & a_{22} - \alpha \end{vmatrix}$$

$$= (a_{11} - \alpha)(a_{22} - \alpha) - a_{12}a_{21}$$

$$= \alpha^2 - \underbrace{(a_{11} + a_{22})}_{2C}\alpha + \underbrace{(a_{11}a_{22} - a_{12}a_{21})}_{D} = 0$$

$$\Rightarrow \alpha_{1,2} = C \pm \sqrt{C^2 - D} \ .$$

(E) In order to find the corresponding eigenvectors we have to look at

$$M_2 \vec{h}_k = \alpha_k \vec{h}_k \ .$$

(1) For $\vec{h}_1^{\,T} = (h_{11}, h_{12})$ the matrix equations are

$$h_{11}(a_{11} - \alpha_1) + h_{12}a_{12} = 0$$

$$h_{11}a_{21} + h_{12}(a_{22} - \alpha_1) = 0$$

Setting $h_{11} = 1$, the first equation yields $h_{12} = \dfrac{\alpha_1 - a_{11}}{a_{12}}$, which also satisfies the second equation.

(2) In an analogous manner, we obtain for $\vec{h}_2^{\,T} = (h_{21}, h_{22}) = \left[1, \dfrac{\alpha_2 - a_{11}}{a_{12}}\right]$.

(F) Using $\Delta T_1(t=0) = \Delta T_2(t=0) = 2.43^\circ\mathrm{C}$ as the initial conditions, we have to solve

$$c_1 + c_2 = 2.43^\circ\mathrm{C}$$

$$c_1 \frac{\alpha_1 - a_{11}}{a_{12}} + c_2 \frac{\alpha_2 - a_{22}}{a_{12}} = 2.43^\circ\mathrm{C} \ .$$

Solving the first equation for c_1 and inserting it into the second equation yields

$$c_2 = 2.43^\circ\mathrm{C}\,\frac{a_{12} - \alpha_1 + a_{11}}{\alpha_2 - \alpha_1} = 0.31^\circ\mathrm{C}$$

and thus

$$c_1 = 2.11^\circ\mathrm{C}$$

where

$$a_{11} = -\frac{\lambda_1 - \gamma f_1}{R_1} = -0.529\,\frac{1}{y}$$

$$a_{12} = \frac{\gamma f_2}{R_1} = 0.221\,\frac{1}{y}$$

$$\alpha_{1,2} = C \pm \sqrt{C^2 - D}$$

↑
App. D

$$= \frac{a_{11} + a_{22}}{2} \pm \sqrt{(a_{11} + a_{22})^2/4 - (a_{11}a_{22} - a_{12}a_{21})}$$

$$= \frac{a_{11} + a_{22}}{2} \pm \sqrt{(a_{11} - a_{22})^2/4 + a_{12}a_{21}}$$

$$= -\frac{\lambda_1 - \gamma f_1}{2R_1} - \frac{\lambda_2 - \gamma f_2}{2R_2}$$

$$\pm \left\{ \left[-\frac{\lambda_1 - \gamma f_1}{2R_1} + \frac{\lambda_2 - \gamma f_2}{2R_2} \right]^2 + \frac{\gamma^2 f_1 f_2}{R_1 R_2} \right\}^{\frac{1}{2}}$$

using $\lambda_1 = \lambda_2$, $f_1 = f_2 = \frac{1}{2}$

$$= \left[\frac{\gamma}{4} - \frac{\lambda_1}{2} \right] \left[\frac{1}{R_1} + \frac{1}{R_2} \right] \pm \left\{ \left[\left[\frac{\gamma}{4} - \frac{\lambda_1}{2} \right] \left[\frac{1}{R_1} - \frac{1}{R_2} \right] \right]^2 + \frac{\gamma^2}{4R_1R_2} \right\}^{\frac{1}{2}}$$

inserting the remaining parameters

$$= -0.458\frac{1}{y} \pm \left\{0.005\frac{1}{y^2} + 0.036\frac{1}{y^2}\right\}^{\frac{1}{2}}$$

$$= -0.458\frac{1}{y} \pm 0.202\frac{1}{y} = \begin{cases} -0.256\dfrac{1}{y} \\ \\ -0.659\dfrac{1}{y} \end{cases} .$$

(G) In case both hemispherical thermal inertias are equal, $R_1 = R_2\ (= R_0)$, our hemispherical transient temperature responses can be directly compared with those of North *et al.* (1981). Because $a_{11} = a_{22}$ and $a_{12} = a_{21}$ (see Eq. (37)), our solutions reduce to the global solution as given by Eq. (26) (or Eq. (27), respectively)

$$\Delta T_1(t) = \Delta T_2(t) = 2.43^\circ\mathrm{C}\, e^{-\frac{B}{R_0}t}$$

$$= 2.43^\circ\mathrm{C}\, e^{-0.260\frac{1}{y}t} .$$

Here

$$\alpha_{1,2} = a_{11} \pm a_{12} = \frac{\lambda_1 - \frac{\gamma}{2} \mp \frac{\gamma}{2}}{R_0} = \begin{cases} -\dfrac{B}{R_0} \\ \\ -\dfrac{B+\gamma}{R_0} \end{cases}$$

(see Eqs. (41a), (41b), (37)),

$$\vec{h}_1{}^T = (1,1) \ , \quad \vec{h}_2{}^T = (1,-1)$$

(see Eqs. (44a), (44b)), and $\Delta T_1(t=0) = \Delta T_2(t=0) = 2.43^\circ\mathrm{C}$ which implies $c_1 = 2.43^\circ\mathrm{C}$ and $c_2 = 0$ (*cf. Appendix F*), i.e., the second relaxation process $(e^{\alpha_2 t})$ is suppressed.

On the other hand the equation to solve, which North *et al.* (1981) are giving, is

$$D\Delta T_m(t) + \frac{B+\gamma-\delta_{0,m}\gamma}{R_0}\Delta T_m(t) = 0$$

where the temperature changes are expressed by Legendre polynomials

$$\Delta T(t,x) = \sum_{m(\mathrm{even})} \Delta T_m(t) P_m(x) \ .$$

Each term in this expansion contains information pertaining to smaller and smaller spatial scales. The first few terms give us the gross features of the planetary climate. $\Delta T_0(t)$ is the planetary average; $\frac{3}{2}\Delta T_2(t)$ is a rough measure of the pole–to–equator difference in temperature change; higher-order terms reveal features at finer spatial scales.

Their general solution is given by

$$\Delta T_m(t) \sim e^{-\frac{B+\gamma-\delta_{0,m}\gamma}{R_0}t},$$

i.e., our solutions $(e^{\alpha_1 t}, e^{\alpha_2 t})$ are in agreement with the first two modes $(m = 0, 2)$. Note that since we consider the earth as being hemispherically symmetrized (because of $R_1 = R_2$), only $\Delta T_0(t)$ of the expansion is retained (the first mode is sufficient to describe a uniform earth) and all the higher modes are suppressed.

The method of solving energy balance equations by introducing a Legendre polynomial expansion for the temperature as proposed by North *et al.* (1981), does not seem to give good access to the latitudinal feedback parameter λ_i, if one wishes to study them in detail. This is because the system of equations represented by Eq. (2) is solved for all indices i simultaneously, thereby making use of a meridional integration process. This results in a globally averaged λ_i.

REFERENCES

Bolz, R.E. and G.L. Tuve. 1973. *Handbook of Tables for Applied Engineering Science* (2nd edition). CRC Press, Cleveland, Ohio.

Budyko, M.I. 1969. The effect of solar radiation variations on the climate of the earth. *Tellus* **21**(5):611–619.

Cess, R.D. 1976. Climate change: An appraisal of atmospheric feedback mechanisms employing zonal climatology. *J. Atmos. Sci.* **33**(10):1831–1843.

de Haan, B.J. 1991. Personal communication. RIVM.

den Elzen, M.G.J. and B.J. de Haan. 1991. A Simple Zonally Energy Balance Model Coupled to a Two-Dimensional Advective–Deep Ocean Model. Paper presented at the Climatic Research Unit, University of East Anglia, Norwich, U.K.

den Elzen, M.G.J. and J. Rotmans. 1991. The socio-economic impact of sea level rise on The Netherlands'. Climatic Change (in press).

den Elzen, M.G.J. and J. Rotmans. 1991. *Modeling Feedback Mechanisms in the Carbon Cycle: Balancing the Carbon Budget.* Submitted to Tellus.

Dickinson, R.E. 1982. Modeling climate changes due to carbon dioxide increases. Pages 101–133 in W.C. Clark (ed.), *Carbon Dioxide Review.* Oxford University Press, New York.

Dickinson, R.E. 1986. How will climate change? Pages 206–270 in B. Bolin, B.R. Döös, J. Jäger, and R.A. Warrick (eds.), *The Greenhouse Effect, Climatic Change, and Ecosystems.* SCOPE 29. John Wiley and Sons, Chichester, U.K.

Ellis, J.S. and T.H. Vonder Haar. 1976. Zonal average earth radiation budget measurements from satellites for climate studies. Atmos. Sci. Pap. 240. Colorado State University, Fort Collins, Colorado.

Gal-Chen, T. and S.H. Schneider. 1976. Energy balance climate modeling: Comparison of radiative and dynamic feedback mechanisms. *Tellus* **28**:108–121.

Hansen, J., I. Fung, A. Lacis, D. Rind, S. Lebedeff, R. Ruedy, G. Russel, and P. Stone. 1988. Global climate changes as forecast by Goddard Institute for Space Studies' three-dimensional model. *J. Geophys. Res.* **93**:9341–9364.

Harvey, L.D.D. 1988. A semianalytic energy balance climate model with explicit sea ice and snow physics. *J. Climate* **1**:1065–1085.

Held, I.M. and M.J. Suarez. 1974. Simple albedo feedback models of the ice caps. *Tellus* **26**:613–629.

Henderson-Sellers, A. and K. McGuffie. 1987. *A Climate Modelling Primer.* John Wiley and Sons, Chichester, U.K.

IPCC. 1990. *Climate Change: The IPCC Scientific Assessment.* Report prepared for the Intergovernmental Panel on Climate Change by Working Group 1. J.T. Houghton, G.J. Jenkins, and J.J. Ephraums (eds.), Cambridge University Press, Cambridge, U.K.

Leemans, R. 1989. Possible changes in natural vegetation cycles due to a global warming. Pages 105–122 in A. Hackl (ed.), *Der Treibhauseffekt: Das Problem – Mögliche Folgen – und erforderliche Maßnahmen.* Akademie für Umwelt und Energie, A–2361 Laxenburg, Austria.

Lian, M.S. and R.D. Cess. 1977. Energy-balance climate models: A reappraisal of ice-albedo feedback. *J. Atmos. Sci.* **34**:1058–1062.

Lindzen, R.S. and B. Farrell. 1977. Some realistic modifications of simple climate models. *J. Atmos. Sci.* **34**:1487–1501.

Nilsson, S., O. Sallnäs, and P. Duinker. 1991. *Forest Potentials and Policy Implications: A Summary of a Study of Eastern and Western European Forests by the International Institute for Applied Systems Analysis.* Executive Report ER–17. International Institute for Applied Systems Analysis, Laxenburg, Austria.

North, G.R. 1975a. Analytical solution to a simple climate model with diffusive heat transport. *J. Atmos. Sci.* **32**:1301–1307.

North, G.R. 1975b. Theory of energy-balance climate models. *J. Atmos. Sci.* **32**(11):2033–2043.

North, G.R. and J.A. Coakley. 1978. Simple seasonal climate models. *Meteorol. Gidrol.* **5**:26–32.

North, G.R. and J.A. Coakley. 1979. Differences between seasonal and mean annual energy balance model calculations of climate and climate sensitivity. *J. Atmos. Sci.* **36**:1189–1204.

North, G.R., R.F. Cahalan, and J.A. Coakley. 1981. Energy balance climate models. *Rev. Geophys. Space Phys.* **19**:91–121.

Pontryagin, L.S. 1962. *Ordinary Differential Equations.* Addison–Wesley Publishing Co., Reading, Massachusetts.

Ramanathan, V., M.S. Lian, and R.D. Cess. 1979. Increased atmospheric CO_2: Zonal and seasonal estimates of the effect on the radiation energy balance and surface temperature. *J. Geophys. Res.* **84**(C8):4949–4958.

Rotmans, J. 1990. *IMAGE: An Integrated Model to Assess the Greenhouse Effect.* Kluwer Academic Publishers, Dordrecht, The Netherlands.

Schlesinger, M.E. 1986. Equilibrium and transient climatic warming induced by increased atmospheric CO_2. *Climate Dynamics* **1**:35–51.

Schneider S.H. and S.L. Thompson. 1981. Atmospheric CO_2 and climate: Importance of the transient response. *J. Geophys. Res.* **86**(C4):3135–3147.

Sellers, W.D. 1969. A global climatic model based on the energy balance of the earth–atmosphere system. *J. Appl. Meteor.* **8**:392–400.

Siegenthaler, U. and H. Oeschger. 1984. Transient temperature changes due to increasing CO_2 using simple models. *Annals of Glaciology* **5**:153–159.

Thompson, S.T. and S.G. Warren. 1982. Parameterization of outgoing infrared radiation derived from detailed radiative calculations. *J. Atmos. Sci.* **39**:2667–2680.

Vonder Haar, T.H. and J.S. Ellis. 1975. Albedo of the cloud-free earth–atmosphere system. *Collection of Abstracts, Second Conference on Atmospheric Radiation*, Arlington, Va., 29–31 October 1975. Amer. Meteor. Soc., 107–110.

Warren, S.G. and S.H. Schneider. 1979. Seasonal simulation as a test for uncertainties in the parameterizations of a Budyko–Sellers zonal climate model. *J. Atmos. Sci.* **36**:1377–1391.

Wigley, T.M.L. 1987. Relative contributions of different trace gases to the greenhouse effect. *Climate Monitor* **16**(1):14–28.

Wigley, T.M.L. and S.C.B. Raper. 1987. Thermal expansion of seawater associated with global warming. *Nature* **330**:127–131.

Wigley, T.M.L. and M.E. Schlesinger. 1985. Analytical solution for the effect of increasing CO_2 on global mean temperature. *Nature* **315**:649–652.